

## RESEARCH ARTICLE

# Neuronal deletion of *Gtf2i* results in developmental microglial alterations in a mouse model related to Williams syndrome

Ela Bar<sup>1,2</sup> | Inbar Fischer<sup>3</sup> | May Rokach<sup>3</sup> | Galit Elad-Sfadia<sup>1</sup> |  
Sophie Shirenova<sup>4,5,6</sup> | Omer Ophir<sup>3</sup> | Sari Schokoroy Trangle<sup>1</sup> | Eitan Okun<sup>4,5,6</sup> |  
Boaz Barak<sup>1,3</sup> 

<sup>1</sup>The School of Psychological Sciences, Faculty of Social Sciences, Tel Aviv University, Tel Aviv, Israel

<sup>2</sup>The School of Neurobiology, Biochemistry & Biophysics, Faculty of Life Sciences, Tel Aviv University, Tel Aviv, Israel

<sup>3</sup>The Sagol School of Neuroscience, Tel Aviv University, Tel Aviv, Israel

<sup>4</sup>The Leslie and Susan Gonda Multidisciplinary Brain Research Center, Bar-Ilan University, Ramat Gan, Israel

<sup>5</sup>The Paul Feder Laboratory on Alzheimer's Disease Research, Bar-Ilan University, Ramat Gan, Israel

<sup>6</sup>The Mina and Everard Goodman Faculty of Life Sciences, Bar-Ilan University, Ramat Gan, Israel

## Correspondence

Eitan Okun, The Leslie and Susan Gonda Multidisciplinary Brain Research Center, Bar-Ilan University, Ramat Gan, Israel.  
Email: [eitan.okun@biu.ac.il](mailto:eitan.okun@biu.ac.il)

Boaz Barak, The School of Psychological Sciences, Faculty of Social Sciences, Tel Aviv University, Tel Aviv, Israel.  
Email: [boazba@tauex.tau.ac.il](mailto:boazba@tauex.tau.ac.il)

## Funding information

The National institute for psychobiology in Israel; Autour des Williams; Williams France Federation; Israel Science Foundation, Grant/Award Number: 2305/20

## Abstract

Williams syndrome (WS) is a genetic neurodevelopmental disorder caused by a heterozygous microdeletion, characterized by hypersociability and unique neurocognitive abnormalities. Of the deleted genes, *GTF2I* has been linked to hypersociability in WS. We have recently shown that *Gtf2i* deletion from forebrain excitatory neurons, referred to as *Gtf2i* conditional knockout (cKO) mice leads to multi-faceted myelination deficits associated with the social behaviors affected in WS. These deficits were potentially mediated also by microglia, as they present a close relationship with oligodendrocytes. To study the impact of altered myelination, we characterized these mice in terms of microglia over the course of development. In postnatal day 30 (P30) *Gtf2i* cKO mice, cortical microglia displayed a more ramified state, as compared with wild type (controls). However, postnatal day 4 (P4) microglia exhibited high proliferation rates and an elevated activation state, demonstrating altered properties related to activation and inflammation in *Gtf2i* cKO mice compared with control. Intriguingly, P4 *Gtf2i* cKO-derived microglial cells exhibited significantly elevated myelin phagocytosis *in vitro* compared to control mice. Lastly, systemic injection of clemastine to P4 *Gtf2i* cKO and control mice until P30, led to a significant interaction between genotypes and treatments on the expression levels of the phagocytic marker CD68, and a significant reduction of the macrophage/microglial marker *Iba1* transcript levels in the cortex of the *Gtf2i* cKO treated mice. Our data thus implicate microglia as important players in WS, and that early postnatal manipulation of microglia might be beneficial in treating inflammatory and myelin-related pathologies.

## KEYWORDS

clemastine, *Gtf2i*, microglia, microglial activation, myelin, neurodevelopmental disorders, Williams syndrome

This is an open access article under the terms of the [Creative Commons Attribution-NonCommercial-NoDerivs](https://creativecommons.org/licenses/by-nc-nd/4.0/) License, which permits use and distribution in any medium, provided the original work is properly cited, the use is non-commercial and no modifications or adaptations are made.

© 2024 The Authors. GLIA published by Wiley Periodicals LLC.

## 1 | INTRODUCTION

Williams syndrome (Kozel et al., 2021; Nir & Barak, 2021) (WS) is a genetic neurodevelopmental disorder caused by a heterozygous micro-deletion of ~26–28 genes from the WS critical region and characterized by hyper-sociability and unique neurocognitive abnormalities (Barak & Feng, 2016). Of the deleted genes, *GTF2I* has been linked to hyper-sociability in WS (Chailangkarn et al., 2018; Ophir et al., 2023; Procyshyn et al., 2017; Sakurai et al., 2011). We have recently shown that *Gtf2i* deletion from mouse forebrain excitatory neurons (Ophir et al., 2023) leads to mitochondrial dysfunction (Nir Sade et al., 2023) and multi-faceted myelination deficits (Barak et al., 2019; Grad et al., 2022; Nir & Barak, 2021) associated with the social behaviors and fine motor skills affected in WS; findings validated in human tissue samples from WS subjects (Barak et al., 2019; Nir & Barak, 2021; Trangle et al., 2023). The myelination-related deficits are mediated by abnormal neuron–glia interactions and have been shown to be ameliorated upon administration of FDA-approved drugs, such as 4-aminopyridine and clemastine (Barak et al., 2019). Clemastine is a first-generation histamine receptor H1 antagonist with a safety profile dictating its use (Liu et al., 2016). Besides its well-known actions as an antihistamine, clemastine also promotes oligodendrocyte precursor cells differentiation into mature oligodendrocytes (OLs) (Liu et al., 2016), myelinating cells of the central nervous system (CNS). Moreover, clemastine alleviates depressive-like behavior by reversing the imbalance in the microglia-related pro-inflammatory state in the mouse hippocampus (Su et al., 2018).

Microglia, the resident innate immune cells of the brain (Aloisi, 2001), are involved in synapse formation and maintenance (Bechade et al., 2013), circuit sculpting (Akiyoshi et al., 2018), myelination (Bennett & Barres, 2017), plasticity (Arnoux & Audinat, 2015), and cognition (Morris et al., 2013). In mice, microglial cells appear before embryonic day 8 (Lichanska & Hume, 2000) and migrate from the yolk sac to the brain via blood circulation (Nayak et al., 2014). These microglia take up residence before differentiation of other CNS cell types to become critical regulators of CNS development (Kierdorf et al., 2013; Ransohoff & Cardona, 2010). As active players during early development, as well as in adulthood, microglia rely on their long processes and unique receptors to directly affect other cells, while indirectly impacting other CNS cells by secreting growth factors (GFs) and cytokines (Olson & Miller, 2004), and via phagocytosis (Tremblay & Sierra, 2014). Upon pathologic stimulation, microglia may change from a ramified to an amoeboid form, secrete inflammation-related factors and phagocytose debris (Aloisi, 2001). Ramified microglia are characterized by extensive branching and are commonly referred to as resting/surveillance microglia (Vidal-Itriago et al., 2022). Various types of receptors expressed on the cell surface of microglia play a crucial role in mediating the phagocytic process. For instance, cluster of differentiation (CD)36 is essential for facilitating the uptake of myelin debris by both macrophages and microglia (Grajchen et al., 2020).

Microglial states are defined by their intrinsic and extrinsic determinants, spatiotemporal context, complexity layers, and ultimately, function (Paolicelli et al., 2022). As a result, different pathologies are

characterized by differential transcriptional signatures and cell-surface marker expression in microglia. Nevertheless, in brain pathologies, microglia can be chronically over-activated, typically resulting in increased Iba1 expression (Norden et al., 2016). Alterations in microglial activity, morphology, gene expression, and protein secretion have been associated with neurodevelopmental disorders (Garey, 2010; Gupta et al., 2014; Tetreault et al., 2012). Increased microglia density was shown in autism spectrum disorder (Morgan et al., 2010), schizophrenia (Garey, 2010), and WS (Wilder et al., 2018). In addition, significant microgliosis was observed in subjects with depression who had committed suicide (Steiner et al., 2008). Impaired synapse refinement was seen in schizophrenia (Sekar et al., 2016), while activated microglia-mediated brain inflammation was observed in attention deficit hyperactivity disorder (Anand et al., 2017) and Tourette syndrome (Lenington et al., 2016). In a mouse model for Tourette syndrome, the reduced number of insulin-like growth factor (IGF)-1-expressing microglia was suggested to mediate neuronal loss (Frick & Pittenger, 2016). A reduction in the expression of inflammatory mediators, such as tumor necrosis factor (TNF)- $\alpha$  and interleukin (IL)-1 $\beta$ , was measured following the administration of IGF-1 (Park et al., 2011), suggesting that IGF-1 has beneficial effects on brain development and metabolism.

In disorders involving myelination deficits, microglia may be compromised in their ability to phagocytose myelin debris and support OLs (Bar & Barak, 2019; Poliani et al., 2015). Microglia were suggested to be involved in the myelin deficits seen in multiple sclerosis, Nasu-Hakola disease (Paloneva et al., 2001) and adult-onset leukoencephalopathy (Arreola et al., 2021; McNamara et al., 2022). Microglia interactions with OLs can affect OL functionality and myelination properties (McNamara et al., 2022; Włodarczyk et al., 2017). Indeed, microglia were shown to have a close relationship with OLs (Bar & Barak, 2019; Domingues et al., 2016), affect myelination (Hamilton & Rome, 1994; Santos & Fields, 2021), influence myelin-related diseases (Olah et al., 2012; Wang et al., 2019) and syndromes (Derecki et al., 2012; Frick & Pittenger, 2016), playing a role in a variety of neurodevelopmental disorders (Bar & Barak, 2019; Kim et al., 2017; Zhan et al., 2014), some of which are mentioned above. Interestingly, in a mouse model of experimental autoimmune encephalomyelitis (EAE), considered an inflammatory disease, microglia present a deactivated, more ramified morphology (Acharjee & Pittman, 2019). Importantly, over-activation of microglia was shown in a complete deletion of the WS critical region mouse model for WS (Ortiz-Romero et al., 2021).

Despite playing crucial roles in myelination, the contributions of microglia to WS remain largely undefined. Considering previous characterization revealed diverse myelin-related deficits in our mouse model at postnatal day 30 (P30) (Barak et al., 2019; Grad et al., 2022; Nir & Barak, 2021) and recognizing the important role microglia play in myelination during the early postnatal stage (Włodarczyk et al., 2017), we conducted further exploration of microglia in this mouse model for WS, both at P30 and at postnatal day 4 (P4). Here, we characterized microglial properties in response to *Gtf2i* deletion from excitatory neurons. We selectively deleted *Gtf2i* in forebrain excitatory neurons alone by crossing *Gtf2i* conditional knockout (cKO) mice (Enkhsandakh

et al., 2016) with Nex-Cre mice (Goebbels et al., 2006) to generate *Gtf2i* cKO mouse model related to WS. We examined microglia along development and found altered microglial properties in these mice. Furthermore, we examined microglial cell-autonomous molecular characteristics *in vitro*, and revealed significantly elevated myelin phagocytosis at P4 *Gtf2i* cKO compared to wild-type mice (controls). We further manipulated microglia function using clemastine, an FDA-approved drug, to better understand its effect on microglia and test a strategy that could potentially assist subjects suffering from inflammatory and myelin-related pathologies.

## 2 | METHODS

### 2.1 | Mice

#### 2.1.1 | Breeding

Mice carrying homozygous *loxP* sites flanking *Gtf2i* were crossed with Nex-Cre mice, a Cre line that carries a Cre recombinase selectively in the excitatory neurons of the forebrain, starting around embryonic day (E) 11.5 (Barak et al., 2019). Nex-Cre mice were background with C57Bl/6 and were previously shown to behave and develop normally (Goebbels et al., 2006). The resulting mice, referred to as cKO (*Gtf2i*<sup>fl/fl</sup>; Nex-Cre<sup>+/+</sup>), have a selective homozygous deletion of *Gtf2i* from the excitatory neurons in the forebrain (Barak et al., 2019). Experiments were carried out exclusively on male mice at the P30 stage. However, the sex of the mice at the P1 and P4 stages was not determined.

#### 2.1.2 | Housing

Each cage contained 2–4 mice of the same sex, regardless of genotype. Mice were housed at 20–24°C under a 12 h light–dark cycle (lights on at 07:00, lights off at 19:00), with food and water available *ad libitum*. All experimental protocols conformed to the guidelines of the Institutional Animal Care and Use Committee of Tel Aviv University, Tel Aviv, Israel. All efforts were made to minimize animal suffering and the number of animals used.

## 3 | GENOTYPING

### 3.1 | DNA extraction

Mice were tagged using an animal micro-tattoo instrument (Fine Scientific Tools, Germany), and a tissue sample from their tail or ear was taken to determine their genotype. To extract genomic DNA, each tissue was suspended in 100  $\mu$ L alkaline lysis buffer (25 mM NaOH (BioLab Ltd., Israel)), and 0.2 mM EDTA (Sigma-Aldrich, Israel) diluted in DDW, pH 12 for 30 min at 95°C while shaking in 600 rpm. To terminate the lysis reaction, 100  $\mu$ L of neutralization buffer (40 mM

Tris–HCl (Sigma-Aldrich, Israel) in DDW, pH 5) were added to the sample, and the mix was cooled at 4°C for at least 5 min.

### 3.2 | Polymerase chain reaction (PCR)

To amplify the specific Cre-recombinase site, 3  $\mu$ L from each preparation was added to each PCR reaction. In addition to the sample, each PCR reaction contained: 12.5  $\mu$ L DreamTaq Green PCR Master Mix (2X) (Thermo Fisher Scientific, USA), 0.5  $\mu$ L of each 3 Nex-Cre primer (1.5  $\mu$ L in total; primers were ordered from Hy-Laboratories (Israel) and diluted to 10 mM according to manufacturer's instructions; for sequences, see Table 1), and 8  $\mu$ L DDW. A C1000 Touch thermal cycler (Bio-Rad Laboratories Ltd., USA) was used under the following conditions: 95°C for 4 min, 30 amplification cycles containing three temperature steps (denaturing at 94°C for 30 s, annealing at 55°C for 30 s, and elongation at 72°C for 1 min), followed by 7 min at 72°C and holding at 4°C until the end.

### 3.3 | Gel electrophoresis

To determine the genotype of the mice, 9  $\mu$ L from each PCR product were inserted into the well of a 2% agarose gel (1x TAE (Bio-Lab, Israel), 2% agarose (Hy Laboratories Inc., Israel) 3% Serva DNA Stain Clear G dye (Serva Electrophoresis GmbH, Germany)) alongside a 100 bp ladder (DM2100 ExcelBand, Smobio Technology, Taiwan). Nex-Cre positive alleles (as expressed in cKO mice) showed two distinct bands (~770 and 525 bp), and Nex-Cre negative alleles (as expressed in *Gtf2i*<sup>fl/fl</sup>;Nex-Cre<sup>-/-</sup> mice; herein referred to as control) showed a single band (~770 bp).

### 3.4 | Sex determination of injected mice

To determine the sex of P4 mice, 3  $\mu$ L from each sample preparation were added to each PCR reaction. In addition to the sample, each PCR reaction contained: 12.5  $\mu$ L DreamTaq Green PCR Master Mix (2X) (Thermo-Fisher, USA), 0.5  $\mu$ L of each primer (primers were ordered from Hy-Laboratories Inc. (Israel) and diluted to 10 mM according to manufacturer's instructions; for sequences, see Table 2) and 8.5 A DDW. A C1000 Touch thermal cycler (Bio-Rad Laboratories Ltd., USA) was used under the following conditions: 94°C for 2 min, 30 amplification cycles containing three temperature steps (denaturing at 94°C for 20 s, annealing at 60°C for 20 s and elongation at

**TABLE 1** PCR primers for cKO or control mouse genotyping.

Name of primer	Sequence
Nex-Cre fwd	GAGTCCTGGAATCAGTCTTTTTTC
Nex-Cre rev	AGAATGTGGAGTAGGGTGAC
Nex-Cre KO	CCGCATAACCACTGAAACAG

**TABLE 2** PCR primers for mouse sex determination.

Name of primer	Sequence
Rmb31x/y fwd	CACCTTAAGAACAAGCCAATACA
Rmb31x/y rev	GGCTTGCTGCTGAAAACATTGG

72°C for 30 s), followed by 5 min at 72°C and holding at 4°C until the end. The PCR product was examined by gel electrophoresis as above. Males presented two bands in gel (sized 269 and 353 bp), while females presented a single band (269 bp). The sex determination primers and protocol were adapted from Tunster (2017).

## 4 | IMMUNOHISTOCHEMISTRY

P4 and P30 mice were perfused with PBS and 4% paraformaldehyde (PFA). Fixed brains were left in PBS for up to 7 days. Using a vibratome (Leica) 100 µm-thick sections were sliced and mounted on slides. Sections were stained using the free-floating method. From each mouse, 2 sections presenting the motor cortex were chosen (approximately bregma 0.78 mm, according to the mouse atlas) and were washed thrice in 1 mL PBS for 5 min each time. Then, the sections were permeabilized with 1.2% Triton X-100 in PBS for 15 min. Following permeabilization, sections were washed in 1 mL PBS (5 min) and blocked with 5% normal goat serum (NGS), 2% bovine serum albumin (BSA), and 0.2% Triton X-100 in PBS for 1 h. The sections were placed in a 96-well plate with 250 µL of a primary antibody solution diluted in a blocking buffer. Anti-Iba1 (1:500, catalog no. 234006, SYSY) and anti-CD68 (1:200, catalog no. 14-0681-82, eBioscience) diluted in blocking buffer (see above) were applied overnight at 4°C. The next day, the sections were washed in 1 mL PBS thrice, 5 min for the first wash and twice for 15 min. Slices were then incubated with secondary antibodies conjugated to Alexa Fluor 488, 555 (1:1000; catalog nos. A11001, A21434; Invitrogen) diluted in blocking buffer for 1 h. Sections were washed in 1 mL PBS thrice, 5 min for the first wash and twice for 15 min. Finally, for the mounting process on glass slides, Vectashield Hardset Antifade Mounting Medium with DAPI (catalog nos. H-1500-10, Vector Laboratories) was used. Images were captured using a Leica SP8 Confocal Laser Scanning Platform. Images were taken at ×20 or ×63 magnifications according to the type of staining. Z-stack images were acquired at 1.2 µm intervals and 1.5 zoom. For analysis, maximum intensity projections were formed from the Z-stacks. Cell numbers and intensity were quantified manually using ImageJ program. CD68 intensity was divided by the number of Iba1<sup>+</sup> cells. Cellular morphology was analyzed using 3DMorph (York et al., 2018).

## 5 | WESTERN BLOT

Brains were dissected from both P4 and P30 mice and homogenized in solubilization buffer (50 mM HEPES pH 7.5, 150 mM NaCl, 10% glycerol, 1% Triton X-100, 1 mM EDTA, pH 8, 1 mM EGTA, pH 8,

1.5 mM MgCl<sub>2</sub>, 200 µM Na<sub>3</sub>PO<sub>4</sub>), protease inhibitor cocktail 1 diluted 1:100 (Merck). Equal amounts of protein from each sample were loaded and resolved by 12.5% SDS-polyacrylamide gel electrophoresis. The separated proteins were electrophoretically transferred to a nitrocellulose membrane in transfer buffer (25 mM Tris-HCl pH 8.3, 190 mM glycine, and 10% (v/v) methanol). Membranes were blocked for 45 min in TBST buffer (0.05 M Tris-HCl, pH 7.5, 0.15 M NaCl, and 0.1% Tween 20) with 6% skim milk for anti-tubulin antibodies and 5% BSA for anti-Iba1 antibodies, blotted overnight with rat anti-Iba1 antibodies (SYSY 234017) or rabbit anti-β-tubulin antibodies (Abcam ab108342) in TBSTX1 buffer, followed by 40 min incubation with a secondary antibody linked to horseradish peroxidase. Immunoreactive bands were detected with an enhanced chemiluminescence reagent. For full blots see Figure S2.

## 6 | CORTEX DISSECTION FOR RNA EXTRACTION

Mice were sacrificed by cervical dislocation and a sample from an ear was taken for genotype verification. Following decapitation, the brain was exposed and placed in a Petri dish containing sterile PBS (Biological Industries, Israel) under an Olympus SZ61 stereo-microscope (Olympus, Japan). Using clean surgical appliances, cortices were cleaned from surrounding tissues (e.g., basal ganglia, blood vessels) and put separately in safe-lock tubes containing 200 µL RNAlater solution (Invitrogen; AB-AM7020) on ice. RNAlater solution was removed following 24 h at 4°C, and the cortices were stored at -80°C until use. All required equipment was sterilized and sprayed with an Rnase inhibitor (Rnase Exitus Plus, Biological Industries, Israel).

## 7 | RNA EXTRACTION AND QUANTITATIVE REVERSE TRANSCRIPTION-POLYMERASE CHAIN REACTION (qRT-PCR)

### 7.1 | RNA extraction and concentration

A stainless steel bead was added to each safe-lock tube containing cortex. After thawing on ice, 500 µL cold TRIzol reagent (Thermo Fisher Scientific) was added, and cortices were homogenized using TissueLyser 2 (Qiagen) for 40 s at 24,000 Hz. After the tissue was fully homogenized, an additional 500 µL of TRIzol was added. After incubation at room temperature (RT) for 5 min, 200 µL of chloroform (Bio-Lab Ltd., Israel) were added to each sample, and tubes were shaken manually for 15 s. Following another incubation at RT for 3 min, the tubes were centrifuged for 20 min at 4°C at 13,800 rpm (Eppendorf Centrifuge 5430R). Once three layers had formed, the top RNA-containing clear layer was carefully transferred to a new tube, to which 1:1 (v/v) isopropanol (Bio-Lab Ltd., Israel) was added to precipitate the RNA. After briefly shaking, the tubes were incubated at RT for 5 min and centrifuged for 15 min at 4°C at 13,800 rpm. Once the RNA had precipitated, the isopropanol was removed, and the pellet

was washed twice with 1 mL of 80% ethanol (Sigma-Aldrich, Israel) mixed with DEPC-treated water (Biological Industries, Israel) and centrifuged after each wash for 5 min at 4°C at 13,800 rpm. After removal of the ethanol, the tubes were left to dry for 15–25 min. Once dry, 35 µL DEPC-treated water was added to each tube, and samples were heated for 5 min at 60°C. RNA concentrations were measured using the Thermo Scientific NanoDrop One device (Thermo Fisher Scientific, USA).

## 7.2 | qRT-PCR

RNA was diluted to a concentration of 200 ng/µl according to the concentration that was measured after RNA extraction. Reverse transcription was performed with random primers and a High-Capacity cDNA Reverse Transcription Kit (Thermo Fisher Scientific, USA). The protocol used with the C1000 Touch thermal cycler (Bio-Rad Laboratories, USA) was 10 min at 25°C, 120 min at 37°C, 5 min at 85°C, and a final step of 4°C. cDNA samples were diluted to 10 ng/µl and stored at –20°C until use.

### 7.2.1 | Real-time PCR

mRNA levels of the different transcripts were determined by real-time PCR using the Fast SYBR Green PCR Master Mix (Thermo Fisher Scientific, USA) and the Bio-Rad CFX Connect Real-Time PCR Detection System (Bio-Rad Laboratories, USA). The program built was 20 s at 95°C, 40 amplification cycles (3 s at 95°C to denature, and 30 s at 60°C for annealing and extending), and a melt curve: 60°C for 5 s, and an increase of 0.5°C every 5 s (including a plate read) until reaching 95°C. mRNA levels were calculated based on the comparative cycle threshold (Ct) method (Schmittgen & Livak, 2008). Normalization of the samples was to the level of glyceraldehyde 3-phosphate dehydrogenase (GAPDH) mRNA, which was also measured. Results are shown as fold change relative to the control group. Primers were constructed and ordered from Hy-Laboratories. The primers were diluted with 10 mM in DEPC-treated water (see sequences in Table 3).

**TABLE 3** RT-PCR primers *Mus musculus* for mRNA quantification.

Origin	Forward	Reverse
<i>Gapdh</i>	GCCTTCCGTGTTCTACC	CCTCAGTGTAGCCCAAGATG
<i>Iba1</i>	TCTGCCGTCCTCAACTTGAAG	GTTTCTCCAGCATTTCGCTTC
<i>CD11b</i>	CTCTTGGCTCTCATCACTGCTG	GCAGCTTCATTATCATGTCTCT
<i>Igf1</i>	CAGCAGCCTTCCAACCTCAATTAT	CGCCAGGTAGAAGAGGTGTGAA
<i>Igfbp3</i>	CTCAAAGCACAGACACCCAGA	ATTCAGTGTGTCTCCATTTCTCT
<i>Igfbp5</i>	TTGCCTCAACGAAAAGAGCTAC	AGTAGGTCTCTTCAGCCATCTCG
<i>CD68</i>	GGACAGCTTACCTTTGGATTCA	AAGGACACATTGTATTCCACCG
<i>Siglech</i>	TCTGTGAGGAAAGGATCTCTGTG	AGAGCACATCACATTGGTAGGAC
<i>Tmem119</i>	GCAGACAGTCAGACCGTCTAGC	AACCAGGGGACCATGTTGAG
<i>Cx3cr1</i>	TGAGCTTTTGCTACTTCCGC	CAAAGACCACAGGAGGATG
<i>Il-1β</i>	CTATGGCAACTGTTCTGAAGTCT	GGTCCGTCACCTTCAAAGAA

## 8 | HYBRIDIZATION CHAIN REACTION (HCR) RNA-FISH

P30 mice were perfused with PBS and brains were extracted and put on dry ice, once frozen, they were moved to –80°C until use. 1 day before sectioning brains were put inside a mold filled with O.C.T (Scigen 4586) and put on dry ice until complete freeze, then moved to –80°C O.N. Using a cryostat (LEICA CM3050 S) 20 µm-thick sections were sliced and mounted on superfrost plus slides (epredia) for 2 days, then HCR protocol applied.

HCR RNA-FISH was performed as thoroughly described here (Choi et al., 2014; Schwarzkopf et al., 2021). A probe for *Iba1* for use with amplifier B4 was purchased from Molecular Instruments. The probe sequence was custom-designed: *Iba1*-AGACGAACCCUCUGAUGUGGUCUGCACAGGGCGCUAGGCUCAGCUCACCCCAUCCUGGAGCAGCCUGCAGACUUAUCCUCUCUCUCCAUCCCGGGGAAAGUCAGCCAGUCCUCCUCAGCUGCCUGUCUUAACCCUGCAUUAUGAAGCCUGAGGAGAUUUAAGUAAACCCUCCCAAGCCCCACCUCAGGAUCUGGGGAAAGCCACUGUCUACCGCAUCCUUGGUUUGAGACAGAAGCUGAUGUGGAAGUGAUGCCUGGGAGUUAAGCAAGGGAAUGAGUGGAAAGGGGAAGUGUGAGAACGGUCCAGAGAGACUGGGGAGCUGGUGGAGAGAGAGACCCAGCGGACAGACUGCCAGCCUAAAGCAACCAGCGUCUGAGGAGCAUAGAGCCAAAGCAGGGAUUUGCAAGGAGGAAAAGCUUUUGGACUGCUGAAGGCCAGCAGGAAGAAGGUCUGGAGGGGAUCAACAAGCAAUCCUCGAUGAUCCCAAUAUCAGCAAUGAUGAGGAUCUGCCGUCCAAACUUGAAGCCUUAAGGUGAAGUACAUGGAGUUUGAUCUGAAUGGAAAUGGAGAUUAUCGAUUAUUGUCCUUGAAGCGAAUGCUGGAGAAACUUGGGUUCCCAAGACCACCUAGAGCUGAAGAGAUUAUUUAGAGAGGUGUCCAGUGGCUCGAGGAGACGUUCAGCUACUCUGACUUUCUCAGAAUGAUGCUGGGCAAGAGAUUCGCAUCUUGAGAAUGAUUCUGAUGUAUGAGGAGAAAACAAGAAACACAAGAGGCCAACUGGUCCCCAGCCAAGAAAGCUAUCUCCGAGCUGCCUGAUUGGAGGUGGAUGUCACACGGUGGGCUGAGUGAGGAGCUUCUGAUGACAGCAGCAUGGAAAAAAGAAACAGUCUGAGCCAGAGUCAGACUAAAUAUUAUGACGCUCUAGUGGGUCA.

Images were captured using a light microscope (IX-83, Olympus). Images were taken at ×20 magnification, and Z-stack images were

acquired at 0.5  $\mu\text{m}$  intervals. For analysis, maximum intensity projections were formed from the Z-stacks. Intensity was quantified manually using ImageJ program.

## 9 | MICROGLIA ISOLATION AND FACS

### 9.1 | Adult microglial isolation

Adult microglia were isolated as previously described (Lau et al., 2021; Moussaud & Draheim, 2010; Nicola et al., 2022) with minor modifications. Briefly, P30 mice were deeply anesthetized and perfused in the left ventricle with PBS. Enzymatic solution (ES) was pre-heated to 37°C. Brains were removed, and cortices were separated and transferred to a freezing tube with 0.5 mL enzymatic solution. Cortices were finely minced with sterile sharp scissors, transferred into tubes with 9.5 mL ES, and shaken in a 37°C incubator shaker (MRC) for 10 min at 60 rpm. Tissues were passed through a 21-gauge needle thrice inside the tubes and returned to the 37°C incubator shaker for 30 min of digestion. Next, cells were centrifuged at 800  $\times$  g at 4°C for 5 min. Then the cell pellet was resuspended in 7 mL working aCSF solution. 3 mL isotonic Percoll was added, and cells were mixed well by inverting 10 times. 2 mL working aCSF was gently added on top.

Cells were centrifuged at 800  $\times$  g at 4°C for 15 min with the slowest acceleration and zero deceleration. Next, the supernatant, including the myelin “ring” formed in the middle of the tube, was removed. The cell pellet was resuspended in 15 mL of DMEM/F12 with 10% FBS (Biological Industries) and 5  $\mu\text{g}/\text{mL}$  GM-CSF (R&D systems) and transferred to a T75 flask in a 37°C 5%  $\text{CO}_2$  incubator. After 14 days, microglia were collected.

### 9.2 | Microglial cell sorting using FACS

To dissociate the tissue into cells, we utilized the “*Adult microglial isolation*” protocol outlined in this section. One whole cortex was harvested for P30 mice, and pooling of two cortices was applied for P4 mice. For P4 samples, the extraction of myelin stage using Percoll was omitted, and instead of perfusing the mice, tissue was treated in red blood cell buffer for 15 min. After staining with Ghost Dye (Neta scientific, #13-0863-T100) for 30 min to detect live cells, centrifugation, washing, and fixation using 2% PFA followed for 20 min. Subsequent steps involved washing with PBS-Triton 0.1%, blocking using FACS buffer (consisting of 2 mg/mL BSA in PBS with added 1:50 normal horse serum) for 15 min, staining with primary intracellular antibodies (Iba1 from SYSY, #234009; CD68 from Abcam, #ab53444; Ki67 from Abcam, #ab15580) in PBST 0.1% (1:200) for 30 min, washing, and staining with ALEXA secondary antibodies (goat anti-Chicken 488, goat anti-Rat 568, and goat anti-Rabbit 647). Subsequent staining involved using CD11b-conjugated antibody (eBioscience, #25-0112-82) at 1:100 in FACS buffer, followed by washing with FACS buffer and centrifuge (all

stages performed on ice and centrifugation at 4°C). Finally, cells were suspended in PBS and analyzed using BD FACSAria™ III Cell Sorter, with data extraction performed using the FlowJo program.

## 10 | MICROGLIA CHARACTERIZATION IN VITRO

### 10.1 | Mixed glial primary culture

Mixed glial cultures were prepared from cortices of P4 cKO and control mice. The mice were decapitated with sterile sharp scissors and the brain was extracted into a new Petri dish with HBSS+HEPES. Digestion of the tissue was performed in a tube using digestion solution, and trituration was then performed using a plating medium containing MEM (BI), FBS, SM1 (Enco), glutamine (Biological Industries), glucose (Sigma), and penicillin–streptomycin (Biological Industries) by pipetting the tissue up and down seven times with a sterile 5 mL pipette. The supernatant was aspirated and centrifuged at 1500 rpm; the pellet was resuspended and seeded into 75cm<sup>2</sup> flasks coated with poly-L-lysine (20  $\mu\text{g}/\text{mL}$ ; Sigma). The cells were cultured at 37°C in humidified 5%  $\text{CO}_2/95\%$  air. After 24 h, the plating medium was replaced with a glial medium containing MEM (Biological Industries), FBS, glucose (Sigma), glutamine (Biological Industries), GlutaMAX (Gibco), and penicillin–streptomycin (Biological Industries). The medium was replaced every three days and confluency was achieved after 8 DIV.

### 10.2 | Microglia isolation using a shaker incubator

Mixed glial cultures were prepared from cortices of P4 cKO and control mice. At 8 DIV, microglia isolation was performed according to the method of Giulian and Baker (Giulian & Baker, 1986) with slight modifications. Microglial cells were obtained by shaking the flasks in a shaker incubator (MRC) for 75 min at 100 rpm, which were then moved to an incubator for 30 min and back to shaking for 1 h at 100 rpm. After mechanical dissociation using the orbital shaker, microglial cells were collected and centrifuged at 1500 rpm. Floating cells were pelleted and stained with trypan blue, and the numbers of live and dead cells were counted using cell counter Countess II (Life Technologies). The cells were then cultured according to different techniques, depending on the experiment. Each culture was prepared from a single mouse.

### 10.3 | Determining the percent of CD11b<sup>+</sup> cells by flow cytometry

The isolated cells were centrifuged at 1500 rpm for 6 min and the medium was extracted. The cell pellet was resuspended in cold PBS containing 1% fetal calf serum. After determining cell number using trypan blue, the diluted cells were transferred into new tubes and Fc-blocker was added for 10 min at 4°C. Next, anti-CD11b-PE was added

to the positive tubes while the same volume of cold PBS was added to the control tubes. All tubes were kept in the dark for 30 min at 4°C. PBS was added to the tubes and after centrifugation was done at 14000 rpm for 5 min, the upper supernatant was extracted, and the pellet of each tube was resuspended with PBS. Cell sorting was performed using a Stratadigm S1000EXi flow cytometer. Data were extracted using the “Flowing software” tool.

## 10.4 | Myelin isolation

The myelin isolation procedure was conducted according to a previously established protocol (Erwig et al., 2019), with minor adjustments. Briefly, mice were sacrificed by cervical dislocation and their cortices were promptly dissected and rapidly frozen using liquid nitrogen. The frozen cortices were then stored at –80°C until further processing. Cortices were then pooled (3 cortices from 3 different control mice) and homogenized in 0.32 M sucrose solution supplemented with protease inhibitor (Catalog no. 539131, Sigma-Aldrich). Samples were then layered onto the top of a 0.85 M sucrose solution to create a sucrose step gradient. Following ultra-centrifugation (Optima XPN80, SW41-Ti rotor, Beckman-Coulter), the crude myelin fraction was visible in the interphase of the sucrose step gradient. Two washing steps were performed with filtered DDW, followed by centrifugation on a second sucrose step gradient to obtain the purified myelin fraction.

## 10.5 | Phagocytosis assay using pHrodo labeled myelin

Primary microglia were isolated from mixed glial cultures and plated in 96-well plates at a density of  $1 \times 10^4$  cells per well. Myelin isolation, as previously outlined (Erwig et al., 2019), was followed by tagging with pHrodo Red SE (Thermo Fisher, # P36600). After an initial 2-day resting period post-isolation, the tagged myelin (25 µg/mL) was introduced into the medium of each well, and phagocytosis activity was imaged every 10 min across 4 fields per well over an 8 h period. The total integrated intensity, defined as the total sum of myelin fluorescent intensity in the entire image, was normalized to cell confluency and analyzed.

## 10.6 | Cell viability assessment using methylene blue

Mitochondrial activity was evaluated by methylene blue (3,7-bis(dimethylamino) phenazathionium chloride; Sigma, #M9140) staining. Microglial culture was fixed using 4% formaldehyde in PBS for 2 h. Then, cells were washed with 0.1 M boric acid for 10 s and 1% methylene blue in 0.1% boric acid was added to the cells for 30 min. The cells were then washed with water thrice, and the remaining color was eluted from the cells using 0.1% HCl. Light absorption was measured by a spectrophotometer at 595 nm.

## 10.6.1 | MTT assay to assess cellular metabolic activity

Isolated microglial cells were seeded  $2.5\text{--}4 \times 10^4$  cells/well into a 24-well plate with the glial medium. After 24 h, the medium was removed, and the cells were incubated with MTT (0.5 mg/mL) diluted in glial medium for 1 h at 37°C. The formazan crystals in the cells were solubilized with DMSO. The level of MTT-formazan was determined by measuring absorbance at 570 nm–630 nm with Tecan absorbance reader (NEOTEC BIO).

## 11 | SYSTEMIC INJECTION OF CLEMASTINE

Experiments were performed on C57BL/6 cKO and control mice (see above). The mice were divided into 4 groups, with 15 mice (before outliers were taken out) in each group: cKO mice placebo, control mice placebo, cKO mice clemastine, and control mice clemastine. Clemastine or PBS was injected i.p. into P4 mice at a concentration of 10 mg/kg every day for 26 days, until P30. Then, the mice were sacrificed using isoflurane and perfused with PBS. Half of the brain was kept in 4% PFA for 2 days and then dissected into 100 µm-thick slices for immunohistochemistry using anti-Iba1 and anti-CD68 antibodies (see above). The other half of the brain was put on a Petri dish and the cortex was isolated and taken for RNA extraction and transcript level analysis (see above).

Images were captured using a light microscope (IX-83, Olympus). Images were taken at  $\times 20$  or  $\times 60$  magnifications, according to the type of staining. Z-stack images were acquired at 0.7 µm intervals and 0.3 intervals, respectively. For analysis, maximum intensity projections were formed from the Z-stacks. Cell numbers and intensity were quantified manually using ImageJ program. CD68 intensity was divided by the number of Iba1<sup>+</sup> cells.

## 12 | STATISTICS AND REPRODUCIBILITY

Data are presented as means  $\pm$  standard error of the mean (SEM), as calculated by GraphPad Prism 8.4.3. Normality of distributions and equality of variances were checked and addressed accordingly using the appropriate statistical analysis.

## 13 | RESULTS

### 13.1 | Reduced proportion of activated microglia in P30 *Gtf2i* cKO mice compared to controls

To associate microglial properties with myelination alterations in *Gtf2i* cKO mice (Barak et al., 2019), we tested microglial properties in P30 *Gtf2i* cKO mice, as compared to controls. Iba1 protein expression was unchanged in the whole cortex (Figure 1a). Microglial numbers in the cortex were quantified by immunostaining for the macrophages/microglial-specific marker Iba1 (Figure 1b), revealing no significant

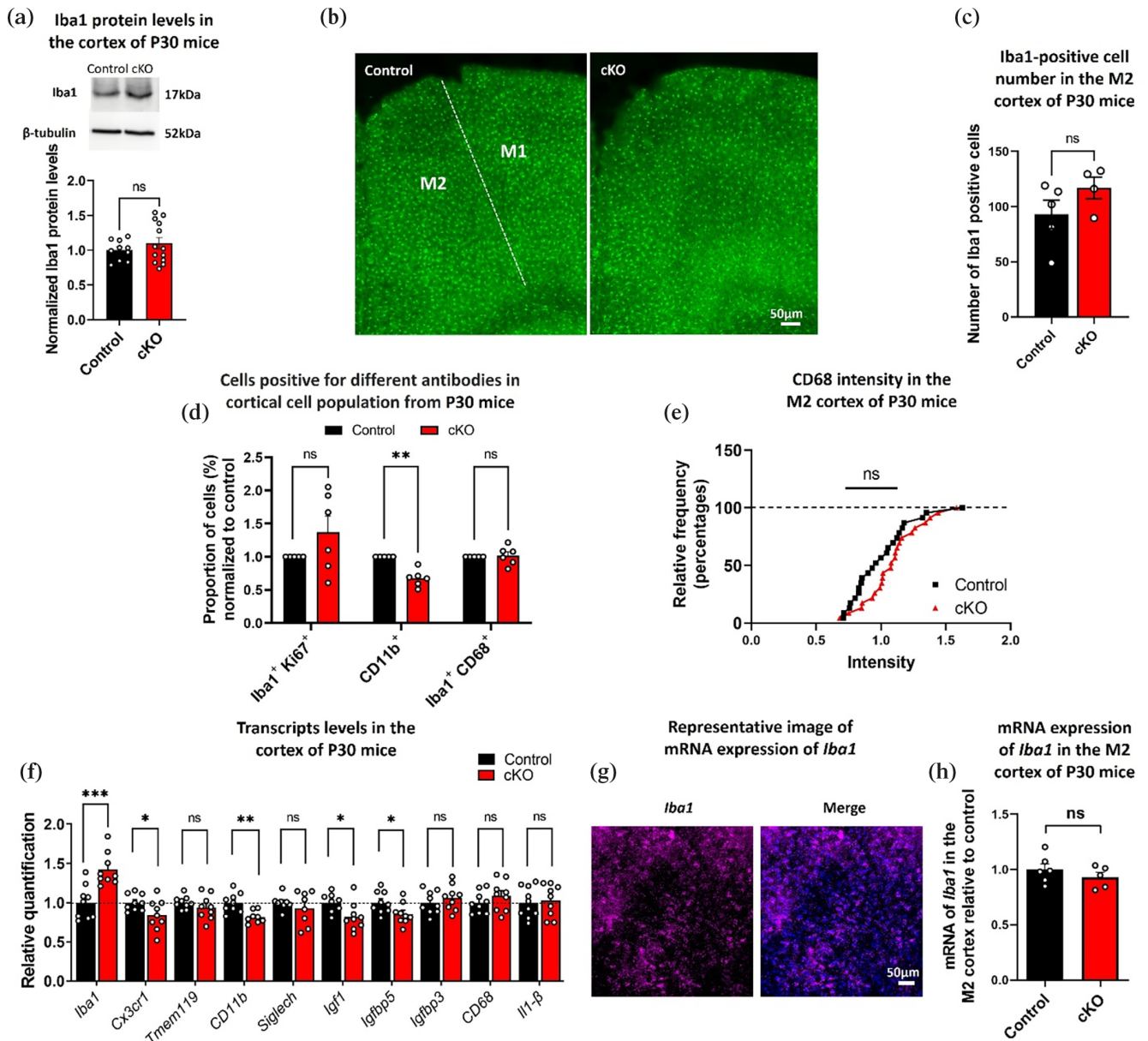


**FIGURE 1** P30 *Gtf2i* cKO mice show a reduced proportion of CD11b<sup>+</sup> population and altered transcription of various genes compared to controls. (a) Iba1 protein levels showed no significant difference in the cortex of *Gtf2i* cKO and control mice, as determined by Western blot. The image was cropped from the full blot. (b) Representative images of Iba1 (green) distribution in a whole coronal section from control (left) and *Gtf2i* cKO mouse (right). The motor cortex (M1 and M2) is marked in white. (c) Iba1<sup>+</sup> cell numbers were unchanged in the M2 cortex of *Gtf2i* cKO mice, as compared to controls. (d) A similar proportion of Iba1<sup>+</sup>Ki67<sup>+</sup> cells, a reduced proportion of CD11b<sup>+</sup> cells, and a comparable proportion of Iba1<sup>+</sup>CD68<sup>+</sup> cells were shown using FACS analysis in the whole cortex of P30 *Gtf2i* cKO mice compared to controls. (e) Cumulative distribution of CD68 intensity divided by the number of Iba1<sup>+</sup> cells. No significant differences were found in the M2 cortex of *Gtf2i* cKO and control mice. (f) Alterations in mRNA levels in the cortex of P30 *Gtf2i* cKO mice, as compared to controls. Significantly increased levels of *Iba1*, decreased levels of *Cx3cr1*, *CD11b*, *Igf1*, and *Igfbp5*, and no significant difference in the levels of *Tmem119*, *Siglech*, *Igfbp3*, *CD68*, and *Il-1 $\beta$*  mRNA were seen in the cortex of P30 *Gtf2i* cKO mice. (g) Representative image of mRNA expression of *Iba1* in magenta (left) and *Iba1* merged with DAPI (right) in the M2 cortex of control mouse. (h) *Iba1* expression showed no significant difference in the M2 cortex of *Gtf2i* cKO and control mice. (a) Statistical significance was determined using an unpaired *t*-test,  $n = 10$  control,  $n = 13$  *Gtf2i* cKO, (c) Unpaired *t*-test,  $n = 5$  control,  $n = 4$  *Gtf2i* cKO. (d) One-sample *t*-test  $n = 5, 6$ . (e) Kolmogorov-Smirnov test,  $n = 6$  in both groups. Slices were analyzed using a confocal microscope at  $\times 63$  magnification with  $1.5\times$  zoom. (f) Unpaired *t*-test, for *Iba1*, *Cx3cr1*, *Tmem119*, *Igfbp3*, *CD68* and *Igfbp5*  $n = 9$  in both groups, *CD11b*,  $n = 9$  control,  $n = 8$  *Gtf2i* cKO, *Igf1*,  $n = 8$  control,  $n = 9$  *Gtf2i* cKO, and for *Il-1 $\beta$*   $n = 10$  control,  $n = 9$  *Gtf2i* cKO. (h) Unpaired *t*-test,  $n = 6$  control,  $n = 5$  *Gtf2i* cKO. Data are shown as means  $\pm$  SEM. ns = nonsignificant  $p > .05$ , \* $p < .05$ , \*\* $p < .01$ , \*\*\* $p < .001$ .

change in P30 *Gtf2i* cKO mice, as compared to controls (Figure 1c). To identify distinct microglial populations, subsequent fluorescence-activated cell sorting (FACS) was conducted using markers for proliferation state (Ki67<sup>+</sup> cells) (Pepe et al., 2017) and activation-related markers (CD11b<sup>+</sup> [Jurga et al., 2020] and CD68<sup>+</sup> [Lier et al., 2021; Wes et al., 2016] cells) in the whole cortex of P30 mice. We observed similarity in the proportion of Iba1<sup>+</sup>Ki67<sup>+</sup> cells, a significantly reduced proportion of CD11b<sup>+</sup> cells, and a comparable proportion of Iba1<sup>+</sup>CD68<sup>+</sup> cells among live cell suspensions in the cortex of P30 *Gtf2i* cKO mice compared to controls (Figure 1d). The distribution of the intensity levels of CD68 was found to be not significantly different in P30 *Gtf2i* cKO mice, as compared to controls (Figure 1e).

### 13.2 | Microglial activation and myelination transcripts are altered in P30 *Gtf2i* cKO mice

We next considered the expression levels of selected microglial activation- and myelination-related transcripts in the cortex of P30 mice (Figure 1f). In contrast to the comparable count of Iba1<sup>+</sup> cells in P30 *Gtf2i* cKO mice, there was a significant upregulation (42%) in *Iba1* transcript levels compared to controls (Figure 1f). *Cx3cr1* and *CD11b* transcript levels were significantly downregulated (16% and 18%, respectively) in P30 *Gtf2i* cKO mice, as compared to controls (Figure 1f). CX3CL1, the ligand for CX3CR1, which is largely expressed in neurons (Tarozzo et al., 2003), is considered a signal for maintaining microglia in the non-activated state (Biber et al., 2007; Cardona et al., 2006). CX3CL1-CX3CR1 signaling thus represents a major communication channel between neurons and microglia, mediating fundamental microglial functions (Limatola & Ransohoff, 2014; Paolicelli et al., 2014). In addition to the reduced proportion of CD11b<sup>+</sup> cells (Figure 1d), as measured by FACS, *CD11b* transcript levels were also significantly decreased in P30 *Gtf2i* cKO mice, as compared to controls (Figure 1f). Transcription of *Igf1*, shown to play a key role in microglia-myelin dynamics (Wlodarczyk et al., 2015; Wlodarczyk et al., 2017), was down-regulated (18%) in P30 *Gtf2i* cKO mice, as compared to controls (Figure 1f). Expression of *Igfbp5*, encoding IGFBP5, a member of the IGFBP family with a strong relationship to IGF-1 (Baxter, 2000), was significantly down-regulated (14%) in the *Gtf2i* cKO mice (Figure 1f).

In light of the significant increase in *Iba1* observed in the cortex of *Gtf2i* cKO mice, and its role in microglial activation and number (Imai & Kohsaka, 2002; Tan et al., 2020), our objective was to determine whether the increase in *Iba1* originated specifically from the M2 cortex. To address this, we utilized Hybridization Chain Reaction (HCR) coupled with RNA fluorescence in situ hybridization (RNA-FISH) (Figure 1g). We observed no significant difference in *Iba1* expression in the M2 cortex of *Gtf2i* cKO mice as compared to controls (Figure 1h).

### 13.3 | Microglia from P30 *Gtf2i* cKO mice are more ramified compared to controls

As changes in microglial morphology could indicate microglial activation state and functionality (Jurga et al., 2020), we adopted a novel

method developed by York et al. (2018). For analyzing microglial morphology. Analysis was performed using the 3DMorph code in MATLAB to assess key morphological characteristics. An example of the analysis and the parameters considered is shown in Figure 2a. We further included a 3D image of a random field, imaged by confocal microscopy, for analysis by the 3DMorph code (Figure 2b). The morphological analysis revealed that microglia in the *Gtf2i* cKO mice exhibited a significantly more ramified morphology, with more processes that were longer and more branched, than did microglia in control mice (Figure 2c).

### 13.4 | In early postnatal *Gtf2i* cKO mice, diverse microglial activation-associated alterations differ from controls

Distinct microglial sub-sets were reported to be related to myelin and normal development at P3–P5 (Wlodarczyk et al., 2017). Given the major role microglia play at early postnatal stage, along with the above-mentioned data from P30 mice, key microglial proteins and their transcripts were next addressed at this developmental stage. Cortical Iba1 protein levels (Figure 3a) and the number of Iba1<sup>+</sup> cells in the M2 cortex (Figure 3b) were significantly increased in P4 *Gtf2i* cKO mice, as compared to controls. Furthermore, using FACS, we observed a significantly higher proportion of Iba1<sup>+</sup>Ki67<sup>+</sup> cells, a non-significant increase in CD11b<sup>+</sup> cells, and a significant decrease in the proportion of Iba1<sup>+</sup>CD68<sup>+</sup> cells in the cortex of P4 *Gtf2i* cKO mice compared to controls (Figure 3c). Accordingly, the distribution of CD68 protein intensity levels in the M2 cortex was also reduced in P4 *Gtf2i* cKO mice compared to controls (Figure 3d).

Consistent with the aforementioned results, *Iba1* levels were also significantly higher in P4 *Gtf2i* cKO mice, as compared to controls (Figure 3e). As opposed to the significant reduction in *Cx3cr1* transcript levels seen in P30 *Gtf2i* cKO mice, relative to controls (Figure 1f), *Cx3cr1* levels were significantly up-regulated (18%) in P4 *Gtf2i* cKO mice, as compared to controls (Figure 3e). White matter-associated microglia were also shown to express reduced levels of homeostatic genes such as *Cx3cr1* and *Tmem119* (Amor et al., 2022), which were increased in our P4 *Gtf2i* cKO mice as compared to controls (Figure 3e). *Siglech*, the product of which promotes phagocytosis (Kopatz et al., 2013) and suppresses pro-inflammatory responses in activated microglia (Konishi et al., 2017), was also significantly up-regulated (18%) in P4 *Gtf2i* cKO mice compared to controls (Figure 3e). *Il-1 $\beta$* , which is considered a marker for neuroinflammation (Rangaraju et al., 2018) was also significantly elevated in P4 *Gtf2i* cKO mice as compared to controls (Figure 3e). The morphological analysis revealed no significant difference in *Gtf2i* cKO mice as compared to controls (Figure 3f).

Next, we aimed to determine if microglia exhibit an altered phagocytosis response to myelin, an endogenous stimulator (Jeon et al., 2008), as we previously reported its impact in WS (Barak et al., 2019; Nir & Barak, 2021). To achieve this, we utilized a previously described method (Erwig et al., 2019) to isolate pure myelin from the mouse brain, and labeled the myelin with pHrodo. This

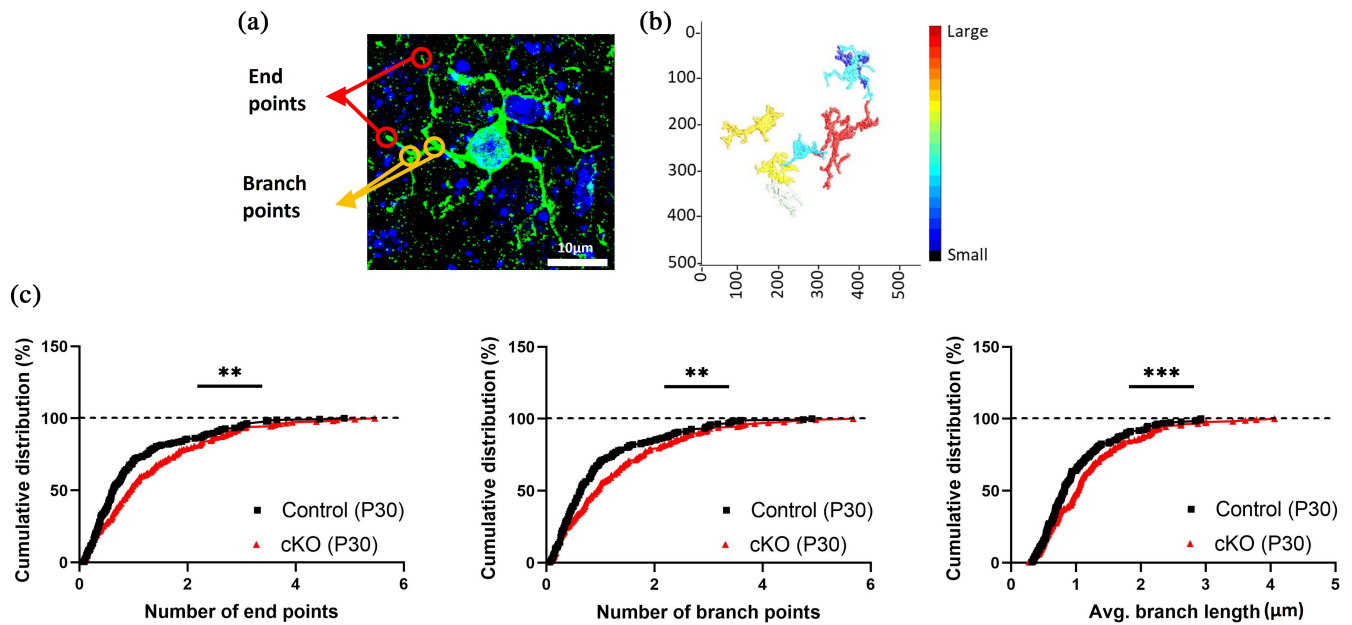


**FIGURE 2** Elevated microglial ramification in P30 *Gtf2i* cKO mice. (a) Immunohistochemistry of Iba1 (green) and DAPI staining (blue) represent some of the parameters analyzed using the 3DMorph code (end points are circled in red and branch points are circled in orange). Iba1 was imaged with a Leica SP8 confocal microscope. The field was taken using a 63 $\times$  objective and 2  $\mu$ m Z-steps through the entire thickness of the tissue. (b) 3D image extracted with the 3DMorph code of York *et al.* (c) Cumulative distribution of the number of end points, number of branch points and average branch length, all were significantly higher in *Gtf2i* cKO mice than in controls. (c) Kolmogorov–Smirnov tests,  $n = 6$  in both groups, were performed to determine statistical significance. Data are shown as means  $\pm$  SEM. \*\* $p < .01$ , \*\*\* $p < .001$ .

fluorescent dye is a pH-sensitive probe that shows low fluorescence intensity at neutral pH but undergoes a significant increase in fluorescence upon acidification within the lysosome (Nicola *et al.*, 2022). Subsequently, we induced *in vitro* phagocytosis using labeled myelin and assessed microglial phagocytic capacity (Nicola *et al.*, 2022; Pluvinaige *et al.*, 2019) using Incucyte. Real-time live-cell imaging allowed us to track the digestion of myelin by microglia over an 8-hour duration. Quantification of fluorescence from the images (Figure 3g and see supporting information) revealed a significant increase in myelin phagocytosis in P4 *Gtf2i* cKO mice compared to controls (Figure 3h).

To study microglia at the earliest postnatal stage, we tested P1 mice. No significant effect was found in microglial characteristics between the tested mice (Figure S1a–c), except for a significant upregulation in the levels of *CD11b* (18%), *Igfbp3* (49%), and *CD68* (44%) in P1 *Gtf2i* cKO mice compared to controls, as seen in Figure S1b. Interestingly, *CD11b* and *CD68*, are both encoding markers related to phagocytosis and activation (Roy *et al.*, 2008; Seabrook *et al.*, 2006).

### 13.5 | Cell-autonomous properties of microglia are similar between *Gtf2i* cKO and control mice

To elucidate the cell-autonomous properties of microglia, we utilized isolated microglia cultures (>94% *CD11b*<sup>+</sup> cells, Figure 4a,b) from the cortices of *Gtf2i* cKO mice and controls at P4. This approach allowed us to study microglia independently, excluding environmental factors

such as endogenous activation by defective myelin or aberrant neuronal activation in the *Gtf2i* cKO mouse model. In these cultures, Tfi-i was similarly expressed in microglia from both *Gtf2i* cKO and control mice (Figure 4c).

To determine microglial cell numbers, microglia were isolated from an 8-day-old primary cell culture prepared from the cortex of P4 *Gtf2i* cKO and control mice. The number of isolated microglia in the cultures was similar in *Gtf2i* cKO mice and their controls (Figure 4d). Microglial mitochondrial perturbations may contribute to neuroinflammation (Feger *et al.*, 2010) by compromising energy production, mitophagy and the release of reactive oxygen species. To explore this, we assessed mitochondrial activity in microglia derived from P4 *Gtf2i* cKO and control mice using the MTT assay which revealed no significant differences (Figure 4e). Subsequently, we examined transcript levels encoding proteins associated with microglial activation and myelination (Figure 4f). Notably, *Iba1* and *CD11b* displayed comparable levels, whereas the expression of *Igfbp5*, encoding an IGF-binding protein, was observed to be reduced in *Gtf2i* cKO mice compared to controls (Figure 4f).

### 13.6 | Clemastine alters microglial activation state

Previous findings from our lab (Barak *et al.*, 2019) showed how clemastine administration ameliorated myelination deficits in *Gtf2i* cKO mice. More recently, clemastine has been shown to directly bind microglial cells (Su *et al.*, 2018; Xie *et al.*, 2020), reducing their

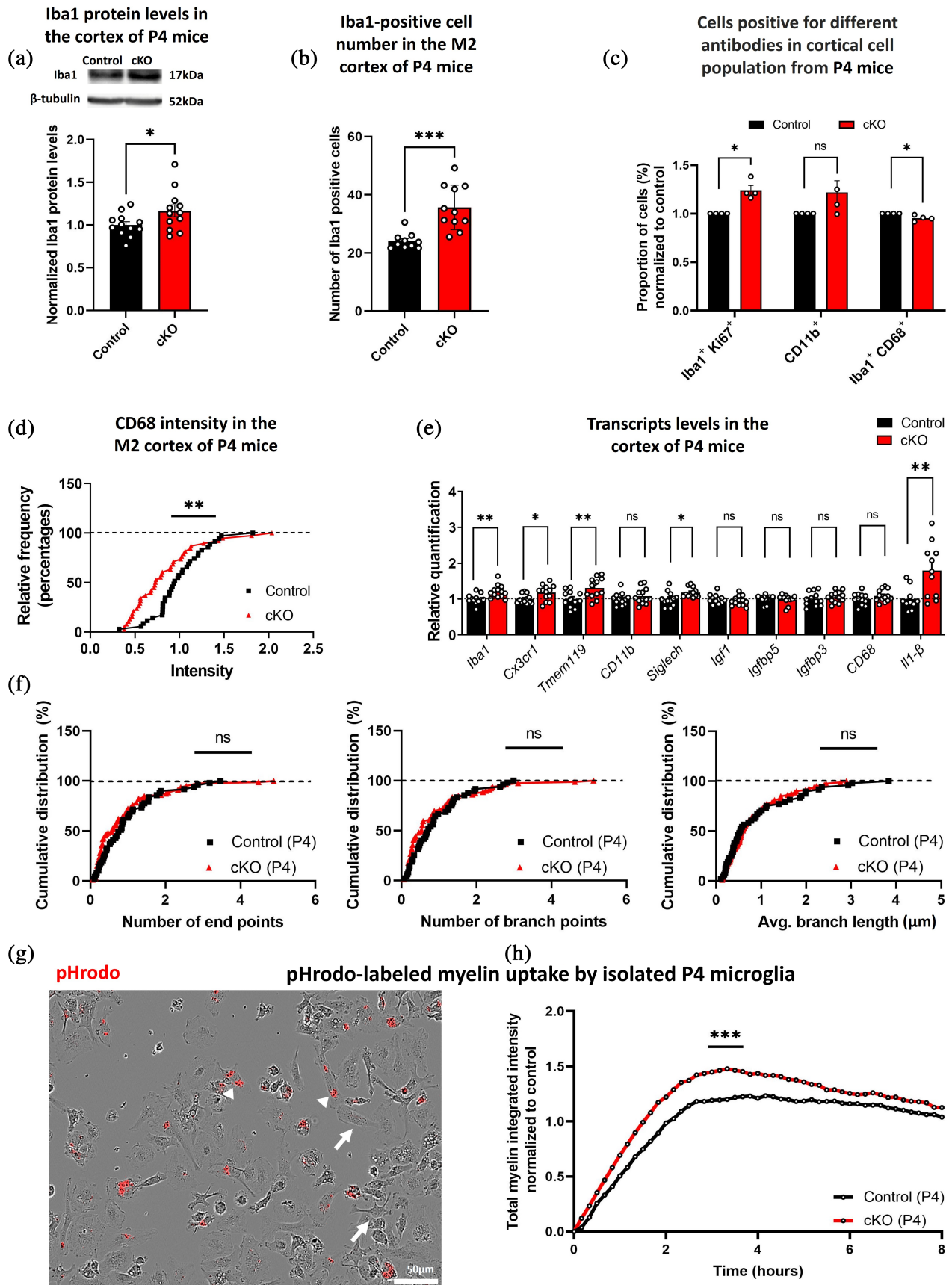


FIGURE 3 Legend on next page.



activation, a process associated with the conversion of oligodendrocyte precursor cells into mature OLs (Su et al., 2018). To study how clemastine administration to a mouse model related to WS affects microglial properties, we administered clemastine daily to mice between P4 and P30. No changes were noted in the number of Iba1<sup>+</sup> cells in the M2 cortex of both *Gtf2i* cKO and control mice, compared to their placebo groups (Figure 5a). CD68 exhibited a significant interaction effect in the M2 cortex between genotypes and treatments (Figure 5b). When assessing *Iba1* transcript levels in whole cortex, we found a significant interaction effect between genotypes and treatments. Post hoc analyses showed a significant decrease of *Iba1* in *Gtf2i* cKO mice following clemastine administration (Figure 5c). No significant change was measured in the expression level of *Cx3cr1* (Figure 5d), *CD11b* (Figure 5e) and *Igf1* (Figure 5f) in both *Gtf2i* cKO and control mice. Measuring *Igfbp5* expression levels revealed a significant interaction effect between treatments (Figure 5g).

### 13.7 | Results summary

In *Gtf2i* cKO mice, an elevation in the number of microglia cells and proliferation was measured during early postnatal stage, when compared to control mice. Under homeostasis, microglia exhibit a more amoeboid morphology during the early postnatal stage (Zusso et al., 2012). Furthermore, there is an upregulation of transcripts associated with activation, phagocytosis, and inflammation, alongside an increased myelin phagocytic capability of myelin *in vitro* during the early postnatal period. This was followed by a more ramified morphology and decreased expression of transcripts associated with activation, phagocytosis and myelination in the young adult mouse model compared to controls (results illustrated in Figure 6). observations align with our *in vivo* findings suggesting potential microglial activation during the early postnatal stage and a subsequent trend toward a more “relaxed” in young-adult *Gtf2i* cKO mice compared to controls.

## 14 | DISCUSSION

In this work, we studied microglia during development in the cortex of a mouse model related to WS in which *Gtf2i* was deleted from fore-brain excitatory neurons and revealed multi-faceted deficits in various properties of microglia. The important role microglia play during the early postnatal stage led us to investigate selected processes related to microglial function during this period. Moreover, previous research demonstrated that a subset of microglia, crucial for normal development and associated with myelination properties, was most abundant at P3–P5 (Włodarczyk et al., 2017), supporting our high interest in studying microglial properties at P4. The possibility of mitigating these deficits was assessed through the administration of clemastine, an FDA-approved drug.

Specifically, our findings show there is a significant microglial proliferation, an additional trait of activation (Green et al., 2022), and a significantly elevated transcripts level involved with activation and inflammation in P4 *Gtf2i* cKO mice, as compared to controls. Furthermore, the proportion of Iba1<sup>+</sup>CD68<sup>+</sup> cells significantly decreased in the cortices, alongside reduced CD68 protein levels in the M2 cortex of P4 *Gtf2i* cKO mice. CD68, a microglial marker located on the lysosomal membrane, is positively associated with activation and phagocytosis (Hopperton et al., 2018; Jurga et al., 2020). Intriguingly, our *in vitro* experiments revealed significantly elevated phagocytosis of pHrodo-labeled myelin while observing a decrease in CD68 within the cortices of P4 *Gtf2i* cKO mice. This discrepancy implies potential compensatory mechanisms or alternative pathways induced by myelin phagocytosis. Additionally, it is essential to consider that *in vitro* phagocytosis lacks the surrounding myelin-defective and impaired neurons found in the *Gtf2i* cKO mouse model which might have a strong effect on microglia examined *in vivo*. Further research is needed to elucidate the specific pathway underlying the increased phagocytosis of myelin in P4 *Gtf2i* cKO mice.

The notable microglial activation at P4 *Gtf2i* cKO mice was succeeded by a significant decline in activation- and myelination-related

**FIGURE 3** P4 *Gtf2i* cKO mice exhibit increased proliferation of microglia, elevated levels of activation-related transcripts, and enhanced phagocytosis compared to controls. (a) Significantly increased levels of Iba1 protein in the cortex of P4 *Gtf2i* cKO mice, as compared to controls, as measured by Western blot. The image was cropped from the full blot. (b) Significantly increased numbers of Iba1<sup>+</sup> cells in the M2 cortex of P4 *Gtf2i* cKO mice, as compared to controls. (c) Significantly increased proportion of Iba1<sup>+</sup>Ki67<sup>+</sup> cells, similar levels of CD11b<sup>+</sup> cells and a significant decrease in Iba1<sup>+</sup>CD68<sup>+</sup> cells were shown using FACS analysis in the whole cortex of P4 *Gtf2i* cKO mice compared to controls. (d) Cumulative distribution of CD68 intensity divided by the number of Iba1<sup>+</sup> cells. A significant decrease was found in the M2 cortex of P4 *Gtf2i* cKO mice, as compared to controls. (e) Alterations in mRNA levels in the cortex of P4 *Gtf2i* cKO mice, as compared to controls. Significant increases in the levels of *Iba1*, *Cx3cr1*, *Tmem119*, *Siglech*, and *Il-1β* transcripts and no significant difference in *CD11b*, *Igf1*, *Igfbp5*, *Igfbp3*, and *CD68* levels were noted in the cortex of P4 cKO mice, as compared to controls. (f) Cumulative distribution of the number of end points, number of branch points, and average branch length showed no significant difference in P4 *Gtf2i* cKO mice compared to controls. (g) Representative image of primary microglia from P4 mouse, showcasing both undigested (white arrows) and digested (white arrowheads) pHrodo-labeled myelin. (h) A significant increase in the intensity levels of pHrodo-labeled myelin was shown in P4 *Gtf2i* cKO mice compared to controls. Statistical significance was determined by (a) an unpaired *t*-test, *n* = 12 in both groups, (b) an unpaired two-tailed *t*-test, *n* = 10 control, *n* = 11 cKO, (c) One-sample *t*-test *n* = 4, (d) Kolmogorov–Smirnov test, *n* = 10 control, *n* = 11 *Gtf2i* cKO, (e) Unpaired *t*-test, for *Iba1*, *Cx3cr1*, *CD11b*, *Igfbp3* and *CD68*, *n* = 12 control, *n* = 13 *Gtf2i* cKO, for *Tmem119*, *Siglech* and *Igfbp5* *n* = 12 in both groups, and for *Il-1β*, *n* = 10 control, *n* = 11 *Gtf2i* cKO, (f) Kolmogorov–Smirnov tests, *n* = 9 control, *n* = 10 *Gtf2i* cKO, (h) Kolmogorov–Smirnov test, *n* = 4 control, *n* = 5 *Gtf2i* cKO. Integrated density defined: Red integrated density per mm<sup>2</sup>/phase area confluence (RCU $\mu$ m<sup>2</sup>/mm<sup>2</sup>) %/normalized to time zero. Data are shown as means  $\pm$  SEM. ns = nonsignificant *p* > .05, \**p* < .05, \*\**p* < .01, \*\*\**p* < .001.

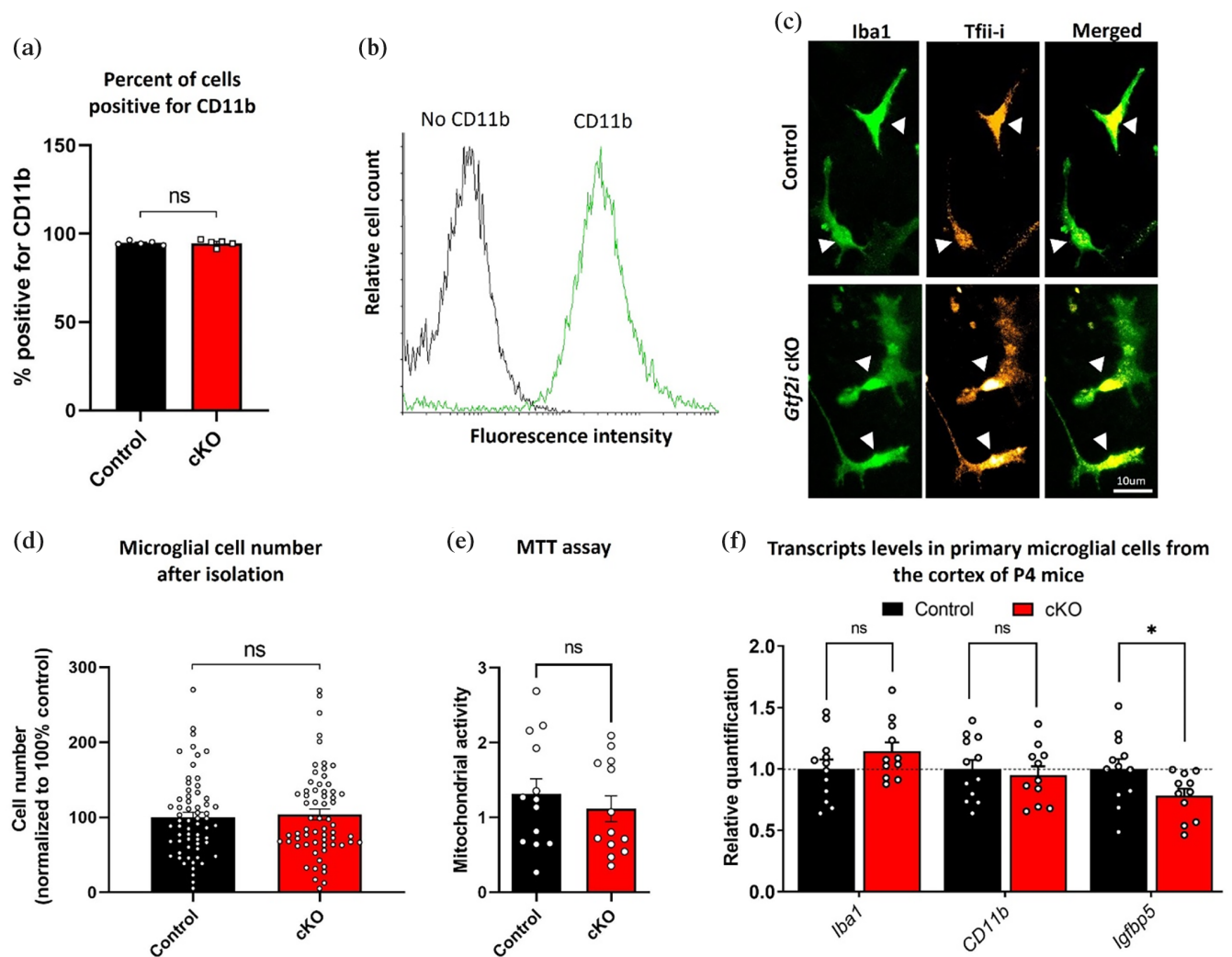


**FIGURE 4** No significant differences in the cell autonomous properties of microglia *in vitro*. (a) Microglial isolation results in >94% microglial cells (CD11b<sup>+</sup>) in primary cultures prepared from both P4 *Gtf2i* cKO and control mice. (b) Representative histogram showing high fluorescence reflecting the amount of CD11b marker in microglial cells isolated from a P4 *Gtf2i* cKO mouse. (c) Immunocytochemistry of microglial cells (15 days *in vitro* (DIV)) from P4 *Gtf2i* cKO and control mice shows Tfii-i in microglial cells (Iba1<sup>+</sup>). (d) No changes in microglial cell numbers were seen following microglial isolation from P4 *Gtf2i* cKO and control mice. (e) The mitochondrial activity of microglial cells in P4 *Gtf2i* cKO mice remained unchanged compared to controls, as assessed by an MTT assay. (f) Analysis of mRNA levels in primary microglial cells from the cortex of P4 *Gtf2i* cKO mice, compared to controls, revealed non-significant differences in *Iba1* and *CD11b* transcripts. However, a significant decrease of 22% was observed in *Igfbp5* transcript levels in microglial cells from the cortex of P4 *Gtf2i* cKO mice compared to controls. (a)  $n = 1$  in both groups, (b)  $n = 5$  in both groups, two-tailed *t*-test, (d)  $n = 62$  control,  $n = 63$  *Gtf2i* cKO, two-tailed Mann-Whitney test, (e) two-tailed *t*-test,  $n = 13$  in both groups, (f) two-tailed *t*-test,  $n = 12$  control,  $n = 11$  *Gtf2i* cKO. Data are shown as means  $\pm$  SEM. ns = non-significant  $p > .05$ , \* $p < .05$ .

transcripts at P30. Additionally, there was a distinct shift toward a significantly more ramified morphology of microglia in young adult mice at P30 *Gtf2i* cKO compared to controls. We also found a significantly reduced proportion of CD11b<sup>+</sup> cells and significantly decreased transcript levels of *Cx3cr1*, *CD11b*, *Igf1*, and *Igfbp5* in P30 *Gtf2i* cKO mice. CD11b is part of complement receptor 3 (CR3), also known as CD11b/CD18 or Mac-1. Which can mediate the phagocytosis of complement-coated myelin (Kopper & Gensel, 2018) and typically serves as an activation marker essential for complement-dependent phagocytosis (Brown & Neher, 2014). The decreased CD11b levels observed in our mutant mice were also found following cuprizone

administration, a condition that leads to demyelination (Remington et al., 2007). This strengthens the interplay between myelination deficits and CD11b.

Notably, reduced CX3CR1 expression was also found in a previous study by our laboratory on post-mortem frontal cortex of subjects with WS compared to typically developed controls (Barak et al., 2019). In that study (Barak et al., 2019), additional microglial transcripts, such as *CCL2*, *VRK2*, and *SELPLG*, were altered. Alterations in the expression of these microglial transcripts may impact myelination (Wlodarczyk et al., 2018), neurodevelopment (Lee et al., 2019) and microglial homeostasis (Masuda et al., 2019), suggesting that

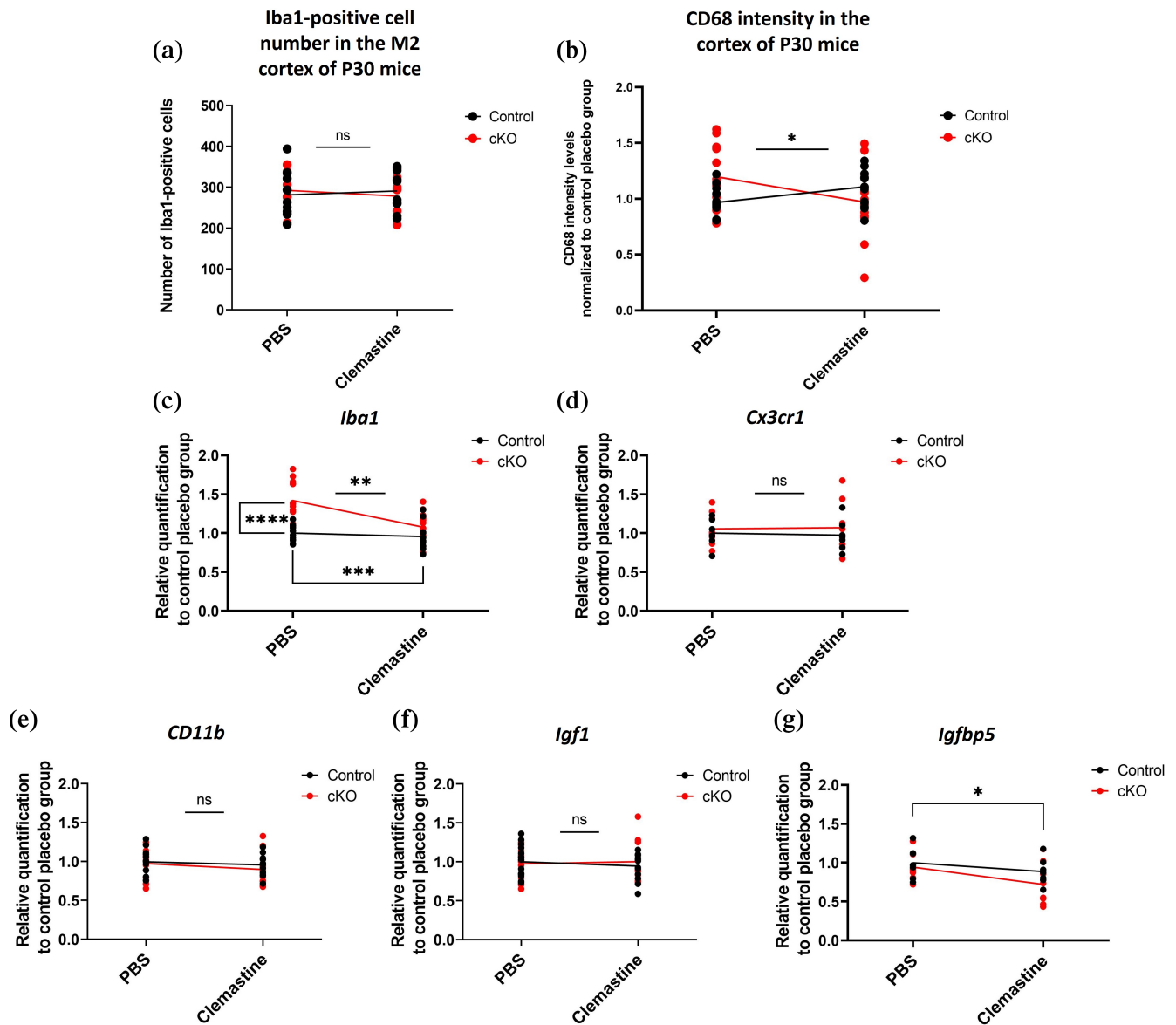


**FIGURE 5** After clemastine administration, CD68, *Iba1* and *Igfbp5* were significantly altered. (a) Unchanged numbers of *Iba1*<sup>+</sup> cells were counted in the M2 cortex of *Gtf2i* cKO and control mice, as compared to each placebo group. (b) CD68 intensity normalized to control placebo group. A significant interaction was found in the M2 cortex of *Gtf2i* cKO mice. (c) Two significant main effects showed reduced mRNA expression level of *Iba1* in *Gtf2i* cKO clemastine group compared to placebo, increased mRNA levels of *Iba1* in cKO mice compared to controls, and an interaction effect. No effects of (d) *Cx3cr1*, (e) *CD11b*, and (f) *Igf1* mRNA were found in the cortex of P30 *Gtf2i* cKO and control mice, as compared to the control placebo group. (g) A significant main effect of *Igfbp5* mRNA levels was shown in clemastine groups compared to placebo groups. Two-way ANOVA followed by a post hoc test. (a)  $n = 14$  control placebo,  $n = 12$  control clemastine,  $n = 10$  *Gtf2i* cKO placebo and  $n = 11$  *Gtf2i* cKO clemastine. (b)  $n = 14$  control placebo and clemastine,  $n = 13$  *Gtf2i* cKO placebo and clemastine. (c)  $n = 13$  control placebo,  $n = 12$  control clemastine,  $n = 13$  *Gtf2i* cKO placebo and clemastine. (d)  $n = 7$  control placebo and clemastine,  $n = 8$  *Gtf2i* cKO placebo and clemastine. (e)  $n = 13$  control placebo and clemastine,  $n = 12$  *Gtf2i* cKO placebo,  $n = 13$  *Gtf2i* cKO clemastine. (f)  $n = 14$  control placebo,  $n = 13$  control clemastine,  $n = 13$  *Gtf2i* cKO placebo and clemastine. (g)  $n = 7$  control placebo and clemastine,  $n = 8$  *Gtf2i* cKO placebo and clemastine. Data are shown as means  $\pm$  SEM. ns = nonsignificant  $p > .05$ ,  $*p < .05$ ,  $**p < .01$ ,  $***p < .001$ ,  $****p < .0001$ .

microglia could contribute to the neurobiological abnormalities observed in WS. IGF1BP5 can modulate IGF-1 directly and determine whether IGF-1 participates in a proliferative or apoptotic pathway (Roschier et al., 2001). *Igfbp5* was shown to play a role in proliferation and apoptosis in the developing brain (Marshman et al., 2003; O'Kusky & Ye, 2012) and to affect cognitive decline and depression (Capuano et al., 2019). Interestingly, in line with our findings at P30, a

study demonstrated a decrease in neuronal expression of both IGF-1 and IGF1BP5 after cerebral hypoxia-ischemia in rats (Lee et al., 1996).

The early postnatal stage is crucial for proper microglial function in myelination processes, among others. We used clemastine to manipulate microglia at this critical stage. Clemastine improved myelination in *Gtf2i* cKO mice (Barak et al., 2019), and since clemastine was previously shown to directly bind microglia and reduce their activation

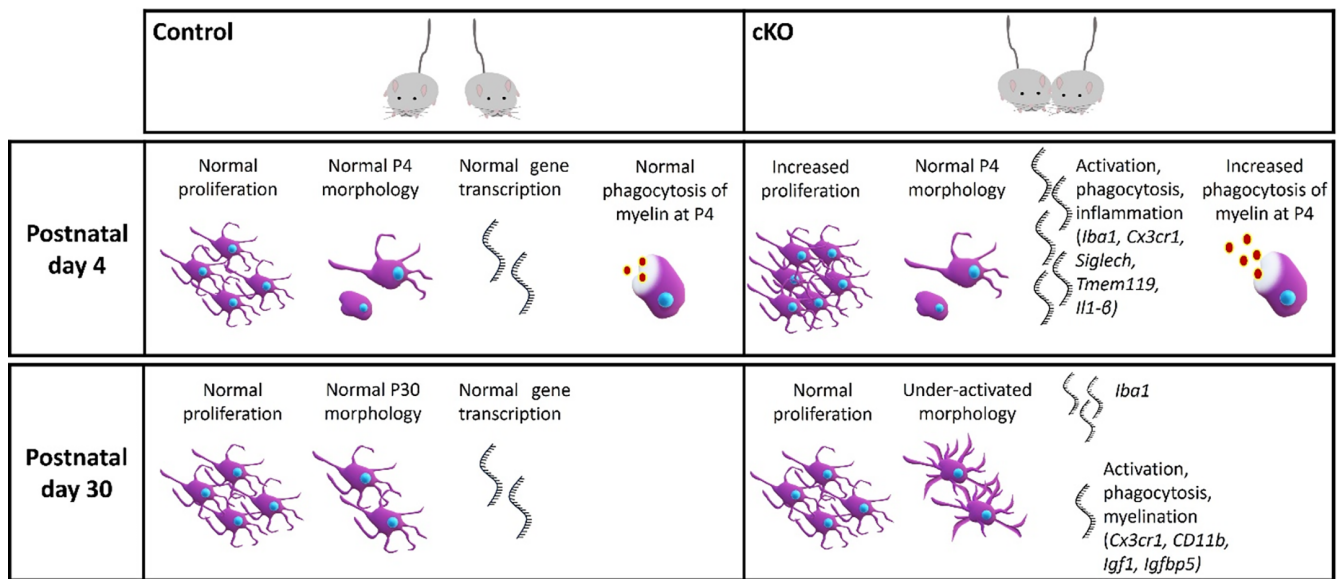


**FIGURE 6** Microglial characteristics throughout development in *Gtf2i* cKO mice. An illustration depicting proliferation, morphology and transcript expression in *Gtf2i* cKO mice compared to control at both P4 and P30, as well as phagocytosis at P4 in *Gtf2i* cKO mice versus control.

(Su et al., 2018; Xie et al., 2020), we systemically injected clemastine from the early postnatal stage until P30 and examined its effects on microglia. In accordance with our findings, *Iba1*<sup>+</sup> cell numbers in the corpus callosum were unchanged after clemastine injection at the postnatal stage (Palma et al., 2022). Interestingly, *Iba1* levels increased after clemastine injection in a mouse model for ALS (Apolloni et al., 2016), although such injection was performed in older mice than in our study (Apolloni et al., 2016). These results reflect how clemastine-mediated effects occur in a development stage-dependent manner.

Furthermore, after clemastine injection, CD68 expression levels showed significant genotypes and treatments interaction effect in the M2 cortex. Post hoc analysis indicated a decrease in CD68 in the M2 cortex of *Gtf2i* cKO mice. This result is compatible with data showing that binding of clemastine to microglia induced an anti-inflammatory effect (Liu et al., 2016; Palma et al., 2022). Moreover, we found that *Iba1* transcript in the whole cortex after clemastine injection showed two significant main effects and a significant interaction effect. Post hoc analysis showed a significant decrease of *Iba1* in *Gtf2i* cKO mice and unchanged levels in controls. Similarly to our findings, in an adult mouse model for stress, *Iba1* protein levels were decreased in the medial prefrontal cortex after systemic clemastine treatment (Su et al., 2018). Remarkably, following clemastine injection, a significant main effect on *Igfbp5* mRNA levels was observed in the clemastine groups compared to the placebo groups. It is noteworthy that *Igfbp5* has been linked to microglial proliferation (Liu et al., 2021). Hence, the decrease in *Iba1* following clemastine injection could potentially contribute to the observed reduction in *Igfbp5* levels. Conversely, the decrease in *Igfbp5* may influence the downregulation of *Iba1*.

To summarize, our data imply that microglia are important players in a WS-related model in which *Gtf2i* is deleted from forebrain excitatory neurons. Whether *Gtf2i* is the only gene that affects microglia in

WS is still unknown. Microglia have been previously recognized as key therapeutic targets in the context of impaired myelin (Lloyd & Miron, 2019; McNamara et al., 2022). Manipulating microglia at the early postnatal stage to treat myelin-related impairments, as shown in this study, may open an avenue that could assist in ameliorating myelination deficits, such as in WS and other neurological conditions involved with myelin pathologies (McNamara et al., 2022). Still, we have recognized in recent years that microglia do not comprise a single homogeneous population. The characteristics of microglia vary between areas of the brain and sometimes even within the same area. Therefore, sub-populations of microglia should be thoroughly investigated, a process that has already begun (Colton, 2009; Grabert et al., 2016; Lawson et al., 1990; Li et al., 2019; Włodarczyk et al., 2017), and population-specific drugs should be developed.

#### AUTHOR CONTRIBUTIONS

Ela Bar, Eitan Okun and Boaz Barak conceptualized and designed the study and wrote the manuscript. Ela Bar, Inbar Fischer, May Rokach, Galit Elad-Sfadia, Sophie Shirenova, Omer Ophir and Sari Schokoroy Trangle collected, analyzed and interpreted the results. All authors reviewed and approved the manuscript.

#### ACKNOWLEDGMENTS

The authors would like to thank the members of the Barak laboratory for their support along the project and Yael Laure for her diligent proofreading and insightful comments on the manuscript. The authors thank Prof. Pablo Blinder, Prof. Dan Frenkel and Prof. Raz Yirmiya for their insightful comments on this study.

#### FUNDING INFORMATION

This research was supported by the Israel science foundation (Grant No. 2305/20, awarded to B.B.), The National Institute of Psychobiology



in Israel (awarded to B.B.), Williams France Federation and Autour des Williams (awarded to B.B.).

## CONFLICT OF INTEREST STATEMENT

The authors declare no conflict of interest.

## DATA AVAILABILITY STATEMENT

All data are included in the manuscript and will be accessible to anyone interested upon request. All materials are commercialized and will be available upon reasonable request.

## ORCID

Boaz Barak  <https://orcid.org/0000-0001-9724-4578>

## REFERENCES

- Acharjee, S., & Pittman, Q. J. (2019). Unexpected microglial "De-activation" associated with altered synaptic transmission in the early stages of an animal model of multiple sclerosis. *Journal of Experimental Neuroscience*, 13, 1179069519825882. <https://doi.org/10.1177/1179069519825882>
- Akiyoshi, R., Wake, H., Kato, D., Horiuchi, H., Ono, R., Ikegami, A., Haruwaka, K., Omori, T., Tachibana, Y., Moorhouse, A. J., & Nabekura, J. (2018). Microglia enhance synapse activity to promote local network synchronization. *eNeuro*, 5, 0088. <https://doi.org/10.1523/ENEURO.0088-18.2018>
- Aloisi, F. (2001). Immune function of microglia. *GLIA*, 36, 165–179. <https://doi.org/10.1002/glia.1106>
- Amor, S., McNamara, N. B., Gerrits, E., Marzin, M. C., Kooistra, S. M., Miron, V. E., & Nutma, E. (2022). White matter microglia heterogeneity in the CNS. *Acta Neuropathologica*, 143, 125–141. <https://doi.org/10.1007/s00401-021-02389-x>
- Anand, D., Colpo, G. D., Zeni, G., Zeni, C. P., & Teixeira, A. L. (2017). Attention-deficit/hyperactivity disorder and inflammation: What does current knowledge tell us? A systematic review. *Frontiers in Psychiatry*, 8, 228. <https://doi.org/10.3389/fpsy.2017.00228>
- Apolloni, S., Fabbriozzi, P., Amadio, S., & Volonte, C. (2016). Actions of the antihistaminergic clemastine on presymptomatic SOD1-G93A mice ameliorate ALS disease progression. *Journal of Neuroinflammation*, 13, 191. <https://doi.org/10.1186/s12974-016-0658-8>
- Arnoux, I., & Audinat, E. (2015). Fractalkine signaling and microglia functions in the developing brain. *Neural Plasticity*, 2015, 689404. <https://doi.org/10.1155/2015/689404>
- Arreola, M. A., Soni, N., Crapser, J. D., Hohsfield, L. A., Elmore, M. R. P., Matheos, D. P., Wood, M. A., Swarup, V., Mortazavi, A., & Green, K. N. (2021). Microglial dyshomeostasis drives perineuronal net and synaptic loss in a CSF1R(+/-) mouse model of ALSP, which can be rescued via CSF1R inhibitors. *Science Advances*, 7, eabg1601. <https://doi.org/10.1126/sciadv.abg1601>
- Bar, E., & Barak, B. (2019). Microglia roles in synaptic plasticity and myelination in homeostatic conditions and neurodevelopmental disorders. *GLIA*, 67, 2125–2141. <https://doi.org/10.1002/glia.23637>
- Barak, B., & Feng, G. (2016). Neurobiology of social behavior abnormalities in autism and Williams syndrome. *Nature Neuroscience*, 19, 647–655. <https://doi.org/10.1038/nn.4276>
- Barak, B., Zhang, Z., Liu, Y., Nir, A., Trangle, S. S., Ennis, M., Levandowski, K. M., Wang, D., Quast, K., Boulting, G. L., Li, Y., Bayarsaihan, D., He, Z., & Feng, G. (2019). Neuronal deletion of Gtf2i, associated with Williams syndrome, causes behavioral and myelin alterations rescuable by a remyelinating drug. *Nature Neuroscience*, 22, 700–708. <https://doi.org/10.1038/s41593-019-0380-9>
- Baxter, R. C. (2000). Insulin-like growth factor (IGF)-binding proteins: Interactions with IGFs and intrinsic bioactivities. *American Journal of Physiology. Endocrinology and Metabolism*, 278, E967–E976. <https://doi.org/10.1152/ajpendo.2000.278.6.E967>
- Bechade, C., Cantaut-Belarif, Y., & Bessis, A. (2013). Microglial control of neuronal activity. *Frontiers in Cellular Neuroscience*, 7, 32. <https://doi.org/10.3389/fncel.2013.00032>
- Bennett, M. L., & Barres, B. A. (2017). A genetically distinct microglial subset promotes myelination. *The EMBO Journal*, 36, 3269–3271. <https://doi.org/10.15252/embj.201798389>
- Biber, K., Neumann, H., Inoue, K., & Boddeke, H. W. (2007). Neuronal 'On' and 'Off' signals control microglia. *Trends in Neurosciences*, 30, 596–602. <https://doi.org/10.1016/j.tins.2007.08.007>
- Brown, G. C., & Neher, J. J. (2014). Microglial phagocytosis of live neurons. *Nature Reviews. Neuroscience*, 15, 209–216. <https://doi.org/10.1038/nrn3710>
- Capuano, A. W., Wilson, R. S., Honer, W. G., Petyuk, V. A., Leurgans, S. E., Yu, L., Gatchel, J. R., Arnold, S., Bennett, D. A., & Arvanitakis, Z. (2019). Brain IGFBP-5 modifies the relation of depressive symptoms to decline in cognition in older persons. *Journal of Affective Disorders*, 250, 313–318. <https://doi.org/10.1016/j.jad.2019.03.051>
- Cardona, A. E., Piro, E. P., Sasse, M. E., Kostenko, V., Cardona, S. M., Dijkstra, I. M., Huang, D. R., Kidd, G., Dombrowski, S., Dutta, R. J., Lee, J. C., Cook, D. N., Jung, S., Lira, S. A., Littman, D. R., & Ransohoff, R. M. (2006). Control of microglial neurotoxicity by the fractalkine receptor. *Nature Neuroscience*, 9, 917–924. <https://doi.org/10.1038/nn1715>
- Chailangkarn, T., Noree, C., & Muotri, A. R. (2018). The contribution of GTF2I haploinsufficiency to Williams syndrome. *Molecular and Cellular Probes*, 40, 45–51. <https://doi.org/10.1016/j.mcp.2017.12.005>
- Choi, H. M., Beck, V. A., & Pierce, N. A. (2014). Next-generation in situ hybridization chain reaction: Higher gain, lower cost, greater durability. *ACS Nano*, 8, 4284–4294. <https://doi.org/10.1021/nn405717p>
- Colton, C. A. (2009). Heterogeneity of microglial activation in the innate immune response in the brain. *Journal of Neuroimmune Pharmacology*, 4, 399–418. <https://doi.org/10.1007/s11481-009-9164-4>
- Derecki, N. C., Cronk, J. C., Lu, Z., Xu, E., Abbott, S. B. G., Guyenet, P. G., & Kipnis, J. (2012). Wild-type microglia arrest pathology in a mouse model of Rett syndrome. *Nature*, 484, 105–109. <https://doi.org/10.1038/nature10907>
- Domingues, H. S., Portugal, C. C., Socodato, R., & Relvas, J. B. (2016). Oligodendrocyte, astrocyte, and microglia crosstalk in myelin development, damage, and repair. *Frontiers in Cell and Development Biology*, 4, 71. <https://doi.org/10.3389/fcell.2016.00071>
- Enkhmandakh, B., Stoddard, C., Mack, K., He, W., Kaback, D., Yee, S. P., & Bayarsaihan, D. (2016). Generation of a mouse model for a conditional inactivation of Gtf2i allele. *Genesis*, 54, 407–412. <https://doi.org/10.1002/dvg.22948>
- Erwig, M. S., Hesse, D., Jung, R. B., Uecker, M., Kusch, K., Tenzer, S., Jahn, O., & Werner, H. B. (2019). Myelin: Methods for purification and proteome analysis. *Methods in Molecular Biology*, 1936, 37–63. [https://doi.org/10.1007/978-1-4939-9072-6\\_3](https://doi.org/10.1007/978-1-4939-9072-6_3)
- Ferger, A. I., Campanelli, L., Reimer, V., Muth, K. N., Merdian, I., Ludolph, A. C., & Witting, A. (2010). Effects of mitochondrial dysfunction on the immunological properties of microglia. *Journal of Neuroinflammation*, 7, 45. <https://doi.org/10.1186/1742-2094-7-45>
- Frick, L., & Pittenger, C. (2016). Microglial dysregulation in OCD, Tourette syndrome, and PANDAS. *Journal of Immunology Research*, 2016, 8606057. <https://doi.org/10.1155/2016/8606057>
- Garey, L. (2010). When cortical development goes wrong: Schizophrenia as a neurodevelopmental disease of microcircuits. *Journal of Anatomy*, 217, 324–333. <https://doi.org/10.1111/j.1469-7580.2010.01231.x>
- Giulian, D., & Baker, T. J. (1986). Characterization of ameboid microglia isolated from developing mammalian brain. *The Journal of Neuroscience*, 6, 2163–2178. <https://doi.org/10.1523/JNEUROSCI.06-08-02163.1986>
- Goebbels, S., Bormuth, I., Bode, U., Hermanson, O., Schwab, M. H., & Nave, K. A. (2006). Genetic targeting of principal neurons in neocortex

- and hippocampus of NEX-Cre mice. *Genesis*, 44, 611–621. <https://doi.org/10.1002/dvg.20256>
- Grabert, K., Michoel, T., Karavolos, M. H., Clohisey, S., Baillie, J. K., Stevens, M. P., Freeman, T. C., Summers, K. M., & McColl, B. W. (2016). Microglial brain region-dependent diversity and selective regional sensitivities to aging. *Nature Neuroscience*, 19, 504–516. <https://doi.org/10.1038/nn.4222>
- Grad, M., Nir, A., Levy, G., Trangle, S. S., Shapira, G., Shomron, N., Assaf, Y., & Barak, B. (2022). Altered White matter and microRNA expression in a murine model related to Williams syndrome suggests that miR-34b/c affects brain development via Ptpu and dcx modulation. *Cell*, 11, 158. <https://doi.org/10.3390/cells11010158>
- Grajchen, E., Wouters, E., van de Haterd, B., Haidar, M., Hardonnière, K., Dierckx, T., van Broeckhoven, J., Erens, C., Hendrix, S., Kerdine-Römer, S., Hendriks, J. J. A., & Bogie, J. F. J. (2020). CD36-mediated uptake of myelin debris by macrophages and microglia reduces neuroinflammation. *Journal of Neuroinflammation*, 17, 224. <https://doi.org/10.1186/s12974-020-01899-x>
- Green, T. R. F., Murphy, S. M., Moreno-Montano, M. P., Audinat, E., & Rowe, R. K. (2022). Reactive morphology of dividing microglia following kainic acid administration. *Frontiers in Neuroscience*, 16, 972138. <https://doi.org/10.3389/fnins.2022.972138>
- Gupta, S., Ellis, S. E., Ashar, F. N., Moes, A., Bader, J. S., Zhan, J., West, A. B., & Arking, D. E. (2014). Transcriptome analysis reveals dysregulation of innate immune response genes and neuronal activity-dependent genes in autism. *Nature Communications*, 5, 5748. <https://doi.org/10.1038/ncomms6748>
- Hamilton, S. P., & Rome, L. H. (1994). Stimulation of in vitro myelin synthesis by microglia. *GLIA*, 11, 326–335. <https://doi.org/10.1002/glia.440110405>
- Hopperton, K. E., Mohammad, D., Trepanier, M. O., Giuliano, V., & Bazinet, R. P. (2018). Markers of microglia in post-mortem brain samples from patients with Alzheimer's disease: A systematic review. *Molecular Psychiatry*, 23, 177–198. <https://doi.org/10.1038/mp.2017.246>
- Imai, Y., & Kohsaka, S. (2002). Intracellular signaling in M-CSF-induced microglia activation: Role of Iba1. *GLIA*, 40, 164–174. <https://doi.org/10.1002/glia.10149>
- Jeon, S. B., Yoon, H. J., Park, S. H., Kim, I. H., & Park, E. J. (2008). Sulfatide, a major lipid component of myelin sheath, activates inflammatory responses as an endogenous stimulator in brain-resident immune cells. *Journal of Immunology*, 181, 8077–8087. <https://doi.org/10.4049/jimmunol.181.11.8077>
- Jurga, A. M., Paleczna, M., & Kuter, K. Z. (2020). Overview of general and discriminating markers of differential microglia phenotypes. *Frontiers in Cellular Neuroscience*, 14, 198. <https://doi.org/10.3389/fncel.2020.00198>
- Kierdorf, K., Erny, D., Goldmann, T., Sander, V., Schulz, C., Perdiguero, E. G., Wieghofer, P., Heinrich, A., Riemke, P., Hölscher, C., Müller, D. N., Luckow, B., Brouwer, T., Debowski, K., Fritz, G., Odenakker, G., Diefenbach, A., Biber, K., Heikenwalder, M., ... Prinz, M. (2013). Microglia emerge from erythromyeloid precursors via Pu.1- and Irf8-dependent pathways. *Nature Neuroscience*, 16, 273–280. <https://doi.org/10.1038/nn.3318>
- Kim, H. J., Cho, M. H., Shim, W. H., Kim, J. K., Jeon, E. Y., Kim, D. H., & Yoon, S. Y. (2017). Deficient autophagy in microglia impairs synaptic pruning and causes social behavioral defects. *Molecular Psychiatry*, 22, 1576–1584. <https://doi.org/10.1038/mp.2016.103>
- Konishi, H., Kobayashi, M., Kunisawa, T., Imai, K., Sayo, A., Malissen, B., Crocker, P. R., Sato, K., & Kiyama, H. (2017). Siglec-H is a microglia-specific marker that discriminates microglia from CNS-associated macrophages and CNS-infiltrating monocytes. *GLIA*, 65, 1927–1943. <https://doi.org/10.1002/glia.23204>
- Kopatz, J., Beutner, C., Welle, K., Bodea, L. G., Reinhardt, J., Claude, J., Linnartz-Gerlach, B., & Neumann, H. (2013). Siglec-h on activated microglia for recognition and engulfment of glioma cells. *GLIA*, 61, 1122–1133. <https://doi.org/10.1002/glia.22501>
- Kopper, T. A.-O., & Gensel, J. C. (2018). Myelin as an inflammatory mediator: Myelin interactions with complement, macrophages, and microglia in spinal cord injury. *Journal of Neuroscience Research*, 96, 969–977. <https://doi.org/10.1002/jnr.24114>
- Kozel, B. A., Barak, B., Kim, C. A., Mervis, C. B., Osborne, L. R., Porter, M., & Pober, B. R. (2021). Williams syndrome. *Nature Reviews. Disease Primers*, 7, 42. <https://doi.org/10.1038/s41572-021-00276-z>
- Lau, S. F., Wu, W., Seo, H., Fu, A. K. Y., & Ip, N. Y. (2021). Quantitative in vivo assessment of amyloid-beta phagocytic capacity in an Alzheimer's disease mouse model. *STAR Protocols*, 2, 100265. <https://doi.org/10.1016/j.xpro.2020.100265>
- Lawson, L. J., Perry, V. H., Dri, P., & Gordon, S. (1990). Heterogeneity in the distribution and morphology of microglia in the normal adult mouse brain. *Neuroscience*, 39, 151–170. [https://doi.org/10.1016/0306-4522\(90\)90229-W](https://doi.org/10.1016/0306-4522(90)90229-W)
- Lee, J., Lee, S., Ryu, Y. J., Lee, D., Kim, S., Seo, J. Y., Oh, E., Paek, S. H., Kim, S. U., Ha, C. M., Choi, S. Y., & Kim, K. T. (2019). Vaccinia-related kinase 2 plays a critical role in microglia-mediated synapse elimination during neurodevelopment. *GLIA*, 67, 1667–1679. <https://doi.org/10.1002/glia.23638>
- Lee, W. H., Wang, G. M., Seaman, L. B., & Vannucci, S. J. (1996). Coordinate IGF-I and IGFBP5 gene expression in perinatal rat brain after hypoxia-ischemia. *Journal of Cerebral Blood Flow and Metabolism*, 16, 227–236. <https://doi.org/10.1097/00004647-199603000-00007>
- Lenington, J. B., Coppola, G., Kataoka-Sasaki, Y., Fernandez, T. V., Palejev, D., Li, Y., Huttner, A., Pletikos, M., Sestan, N., Leckman, J. F., & Vaccarino, F. M. (2016). Transcriptome analysis of the human striatum in Tourette syndrome. *Biological Psychiatry*, 79, 372–382. <https://doi.org/10.1016/j.biopsych.2014.07.018>
- Li, Q., Cheng, Z., Zhou, L., Darmanis, S., Neff, N. F., Okamoto, J., Gulati, G., Bennett, M. L., Sun, L. O., Clarke, L. E., Marschallinger, J., Yu, G., Quake, S. R., Wyss-Coray, T., & Barres, B. A. (2019). Developmental heterogeneity of microglia and brain myeloid cells revealed by deep single-cell RNA sequencing. *Neuron*, 101, 207–223e10. <https://doi.org/10.1016/j.neuron.2018.12.006>
- Lichanska, A. M., & Hume, D. A. (2000). Origins and functions of phagocytes in the embryo. *Experimental Hematology*, 28, 601–611. [https://doi.org/10.1016/S0301-472X\(00\)00157-0](https://doi.org/10.1016/S0301-472X(00)00157-0)
- Lier, J., Streit, W. J., & Bechmann, I. (2021). Beyond activation: Characterizing microglial functional phenotypes. *Cell*, 10, 2236. <https://doi.org/10.3390/cells10092236>
- Limatola, C., & Ransohoff, R. M. (2014). Modulating neurotoxicity through CX3CL1/CX3CR1 signaling. *Frontiers in Cellular Neuroscience*, 8, 229. <https://doi.org/10.3389/fncel.2014.00229>
- Liu, H., Sun, Y., Zhang, Q., Jin, W., Gordon, R. E., Zhang, Y., Wang, J., Sun, C., Wang, Z. J., Qi, X., Zhang, J., Huang, B., Gui, Q., Yuan, H., Chen, L., Ma, X., Fang, C., Liu, Y. Q., Yu, X., & Feng, S. (2021). Pro-inflammatory and proliferative microglia drive progression of glioblastoma. *Cell Reports*, 36, 109718. <https://doi.org/10.1016/j.celrep.2021.109718>
- Liu, J., Dupree, J. L., Gacias, M., Frawley, R., Sikder, T., Naik, P., & Casaccia, P. (2016). Clemastine enhances myelination in the prefrontal cortex and rescues behavioral changes in socially isolated mice. *The Journal of Neuroscience*, 36, 957–962. <https://doi.org/10.1523/jneurosci.3608-15.2016>
- Lloyd, A. F., & Miron, V. E. (2019). The pro-remyelination properties of microglia in the central nervous system. *Nature reviews. Neurology*, 15, 447–458. <https://doi.org/10.1038/s41582-019-0184-2>
- Marshman, E., Green, K. A., Flint, D. J., White, A., Streuli, C. H., & Westwood, M. (2003). Insulin-like growth factor binding protein 5 and apoptosis in mammary epithelial cells. *Journal of Cell Science*, 116, 675–682. <https://doi.org/10.1242/jcs.00263>
- Masuda, T., Sankowski, R., Staszewski, O., Böttcher, C., Amann, L., Sagar, Scheiwe, C., Nessler, S., Kunz, P., van Loo, G., Arnd Coenen, V., Christoph Reinacher, P., Michel, A., Sure, U., Gold, R., Grün, D., Priller, J., Stadelmann, C., & Prinz, M. (2019). Spatial and temporal



- heterogeneity of mouse and human microglia at single-cell resolution. *Nature*, 566, 388–392. <https://doi.org/10.1038/s41586-019-0924-x>
- McNamara, N. B., Munro, D. A. D., Bestard-Cuche, N., Uyeda, A., Bogie, J. F. J., Hoffmann, A., Holloway, R. K., Molina-Gonzalez, I., Askeew, K. E., Mitchell, S., Mungall, W., Dodds, M., Dittmayer, C., Moss, J., Rose, J., Szymkowiak, S., Amann, L., McColl, B. W., Prinz, M., ... Miron, V. E. (2022). Microglia regulate central nervous system myelin growth and integrity. *Nature*, 613, 120–129. <https://doi.org/10.1038/s41586-022-05534-y>
- Morgan, J. T., Chana, G., Pardo, C. A., Achim, C., Semendeferi, K., Buckwalter, J., Courchesne, E., & Everall, I. P. (2010). Microglial activation and increased microglial density observed in the dorsolateral prefrontal cortex in autism. *Biological Psychiatry*, 68, 368–376. <https://doi.org/10.1016/j.biopsych.2010.05.024>
- Morris, G. P., Clark, I. A., Zinn, R., & Vissel, B. (2013). Microglia: A new frontier for synaptic plasticity, learning and memory, and neurodegenerative disease research. *Neurobiology of Learning and Memory*, 105, 40–53. <https://doi.org/10.1016/j.nlm.2013.07.002>
- Moussaud, S., & Draheim, H. J. (2010). A new method to isolate microglia from adult mice and culture them for an extended period of time. *Journal of Neuroscience Methods*, 187, 243–253. <https://doi.org/10.1016/j.jneumeth.2010.01.017>
- Nayak, D., Roth, T. L., & McGavern, D. B. (2014). Microglia development and function. *Annual Review of Immunology*, 32, 367–402. <https://doi.org/10.1146/annurev-immunol-032713-120240>
- Nicola, R., Madar, R., & Okun, E. (2022). HCAR1-mediated L-lactate signaling suppresses microglial phagocytosis. *Neuromolecular Medicine*, 24, 399–404. <https://doi.org/10.1007/s12017-022-08710-5>
- Nir, A., & Barak, B. (2021). White matter alterations in Williams syndrome related to behavioral and motor impairments. *GLIA*, 69, 5–19. <https://doi.org/10.1002/glia.23868>
- Nir Sade, A., Levy, G., Schokoroy Trangle, S., Elad Sfadia, G., Bar, E., Ophir, O., Fischer, I., Rokach, M., Atzmon, A., Parnas, H., Rosenberg, T., Marco, A., Elroy Stein, O., & Barak, B. (2023). Neuronal Gtf2i deletion alters mitochondrial and autophagic properties. *Communications Biology*, 6, 1269. <https://doi.org/10.1038/s42003-023-05612-5>
- Norden, D. M., Trojanowski, P. J., Villanueva, E., Navarro, E., & Godbout, J. P. (2016). Sequential activation of microglia and astrocyte cytokine expression precedes increased Iba-1 or GFAP immunoreactivity following systemic immune challenge. *GLIA*, 64, 300–316. <https://doi.org/10.1002/glia.22930>
- O'Kusky, J., & Ye, P. (2012). Neurodevelopmental effects of insulin-like growth factor signaling. *Frontiers in Neuroendocrinology*, 33, 230–251. <https://doi.org/10.1016/j.yfrne.2012.06.002>
- Olah, M., Amor, S., Brouwer, N., Vinet, J., Eggen, B., Biber, K., & Boddeke, H. W. G. M. (2012). Identification of a microglia phenotype supportive of remyelination. *GLIA*, 60, 306–321. <https://doi.org/10.1002/glia.21266>
- Olson, J. K., & Miller, S. D. (2004). Microglia initiate central nervous system innate and adaptive immune responses through multiple TLRs. *Journal of Immunology*, 173, 3916–3924. <https://doi.org/10.4049/jimmunol.173.6.3916>
- Ophir, O., Levy, G., Bar, E., Kimchi Feldhorn, O., Rokach, M., Elad Sfadia, G., & Barak, B. (2023). Deletion of Gtf2i via systemic administration of AAV-PHP.eB virus increases social behavior in a mouse model of a neurodevelopmental disorder. *Biomedicine*, 11, 2273. <https://doi.org/10.3390/biomed11082273>
- Ortiz-Romero, P., Gonzalez-Simon, A., Egea, G., Perez-Jurado, L. A., & Campuzano, V. (2021). Co-treatment with verapamil and curcumin attenuates the behavioral alterations observed in Williams-Beuren syndrome mice by regulation of MAPK pathway and microglia overexpression. *Frontiers in Pharmacology*, 12, 670785. <https://doi.org/10.3389/fphar.2021.670785>
- Palma, A., Chara, J. C., Montilla, A., Otxoa-de-Amezaga, A., Ruiz-Jaén, F., Planas, A. M., Matute, C., Pérez-Samartín, A., & Domercq, M. (2022). Clemastine induces an impairment in developmental myelination. *Frontiers in Cell and Development Biology*, 10, 841548. <https://doi.org/10.3389/fcell.2022.841548>
- Paloneva, J., Autti, T., Raininko, R., Partanen, J., Salonen, O., Puranen, M., Hakola, P., & Haltia, M. (2001). CNS manifestations of Nasu-Hakola disease: A frontal dementia with bone cysts. *Neurology*, 56, 1552–1558. <https://doi.org/10.1212/WNL.56.11.1552>
- Paolicelli, R. C., Bisht, K., & Tremblay, M. E. (2014). Fractalkine regulation of microglial physiology and consequences on the brain and behavior. *Frontiers in Cellular Neuroscience*, 8, 129. <https://doi.org/10.3389/fncel.2014.00129>
- Paolicelli, R. C., Sierra, A., Stevens, B., Tremblay, M. E., Aguzzi, A., Ajami, B., Amit, I., Audinat, E., Bechmann, I., Bennett, M., Bennett, F., Bessis, A., Biber, K., Bilbo, S., Blurton-Jones, M., Boddeke, E., Brites, D., Bröne, B., Brown, G. C., ... Wyss-Coray, T. (2022). Microglia states and nomenclature: A field at its crossroads. *Neuron*, 110, 3458–3483. <https://doi.org/10.1016/j.neuron.2022.10.020>
- Park, S. E., Dantzer, R., Kelley, K. W., & McCusker, R. H. (2011). Central administration of insulin-like growth factor-I decreases depressive-like behavior and brain cytokine expression in mice. *Journal of Neuroinflammation*, 8, 12. <https://doi.org/10.1186/1742-2094-8-12>
- Pepe, G., de Maglie, M., Minoli, L., Villa, A., Maggi, A., & Vegeto, E. (2017). Selective proliferative response of microglia to alternative polarization signals. *Journal of Neuroinflammation*, 14, 236. <https://doi.org/10.1186/s12974-017-1011-6>
- Pluvinage, J. V., Haney, M. S., Smith, B. A. H., Sun, J., Iram, T., Bonanno, L., Li, L., Lee, D. P., Morgens, D. W., Yang, A. C., Shuken, S. R., Gate, D., Scott, M., Khatri, P., Luo, J., Bertozzi, C. R., Bassik, M. C., & Wyss-Coray, T. (2019). CD22 blockade restores homeostatic microglial phagocytosis in ageing brains. *Nature*, 568, 187–192. <https://doi.org/10.1038/s41586-019-1088-4>
- Poliani, P. L., Wang, Y., Fontana, E., Robinette, M. L., Yamanishi, Y., Gilfillan, S., & Colonna, M. (2015). TREM2 sustains microglial expansion during aging and response to demyelination. *The Journal of Clinical Investigation*, 125, 2161–2170. <https://doi.org/10.1172/JCI77983>
- Procyshyn, T. L., Spence, J., Read, S., Watson, N. V., & Crespi, B. J. (2017). The Williams syndrome prosociality gene GTF2I mediates oxytocin reactivity and social anxiety in a healthy population. *Biology Letters*, 13, 20170051. <https://doi.org/10.1098/rsbl.2017.0051>
- Rangaraju, S., Dammer, E. B., Raza, S. A., Rathakrishnan, P., Xiao, H., Gao, T., Duong, D. M., Pennington, M. W., Lah, J. J., Seyfried, N. T., & Levey, A. I. (2018). Identification and therapeutic modulation of a pro-inflammatory subset of disease-associated-microglia in Alzheimer's disease. *Molecular Neurodegeneration*, 13, 24. <https://doi.org/10.1186/s13024-018-0254-8>
- Ransohoff, R. M., & Cardona, A. E. (2010). The myeloid cells of the central nervous system parenchyma. *Nature*, 468, 253–262. <https://doi.org/10.1038/nature09615>
- Remington, L. T., Babcock, A. A., Zehntner, S. P., & Owens, T. (2007). Microglial recruitment, activation, and proliferation in response to primary demyelination. *The American Journal of Pathology*, 170, 1713–1724. <https://doi.org/10.2353/ajpath.2007.060783>
- Roschier, M., Kuusisto, E., Suuronen, T., Korhonen, P., Kyrlylenko, S., & Salminen, A. (2001). Insulin-like growth factor binding protein 5 and type-1 insulin-like growth factor receptor are differentially regulated during apoptosis in cerebellar granule cells. *Journal of Neurochemistry*, 76, 11–20. <https://doi.org/10.1046/j.1471-4159.2001.00002.x>
- Roy, A., Jana, A., Yatish, K., Freidt, M. B., Fung, Y. K., Martinson, J. A., & Pahan, K. (2008). Reactive oxygen species up-regulate CD11b in microglia via nitric oxide: Implications for neurodegenerative diseases. *Free Radical Biology & Medicine*, 45, 686–699. <https://doi.org/10.1016/j.freeradbiomed.2008.05.026>
- Sakurai, T., Dorr, N. P., Takahashi, N., McInnes, L. A., Elder, G. A., & Buxbaum, J. D. (2011). Haploinsufficiency of Gtf2i, a gene deleted in Williams syndrome, leads to increases in social interactions. *Autism Research*, 4, 28–39. <https://doi.org/10.1002/aur.169>

- Santos, E. N., & Fields, R. D. (2021). Regulation of myelination by microglia. *Science Advances*, 7, eabk1131. <https://doi.org/10.1126/sciadv.abk1131>
- Schmittgen, T. D., & Livak, K. J. (2008). Analyzing real-time PCR data by the comparative C(T) method. *Nature Protocols*, 3, 1101–1108. <https://doi.org/10.1038/nprot.2008.73>
- Schwarzkopf, M., Liu, M. C., Schulte, S. J., Ives, R., Husain, N., Choi, H. M. T., & Pierce, N. A. (2021). Hybridization chain reaction enables a unified approach to multiplexed, quantitative, high-resolution immunohistochemistry and in situ hybridization. *Development*, 148, 22. <https://doi.org/10.1242/dev.199847>
- Seabrook, T. J., Jiang, L., Maier, M., & Lemere, C. A. (2006). Minocycline affects microglia activation, Abeta deposition, and behavior in APP-tg mice. *GLIA*, 53, 776–782. <https://doi.org/10.1002/glia.20338>
- Sekar, A., Bialas, A. R., de Rivera, H., Davis, A., Hammond, T. R., Kamitaki, N., Tooley, K., Presumey, J., Baum, M., van Doren, V., Genovese, G., Rose, S. A., Handsaker, R. E., Schizophrenia Working Group of the Psychiatric Genomics Consortium, Daly, M. J., Carroll, M. C., Stevens, B., & McCarroll, S. A. (2016). Schizophrenia risk from complex variation of complement component 4. *Nature*, 530, 177–183. <https://doi.org/10.1038/nature16549>
- Steiner, J., Bielau, H., Brisch, R., Danos, P., Ullrich, O., Mawrin, C., Bernstein, H. G., & Bogerts, B. (2008). Immunological aspects in the neurobiology of suicide: Elevated microglial density in schizophrenia and depression is associated with suicide. *Journal of Psychiatric Research*, 42, 151–157. <https://doi.org/10.1016/j.jpsychires.2006.10.013>
- Su, W. J., Zhang, T., Jiang, C. L., & Wang, W. (2018). Clemastine alleviates depressive-like behavior through reversing the imbalance of microglia-related pro-inflammatory state in mouse hippocampus. *Frontiers in Cellular Neuroscience*, 12, 412. <https://doi.org/10.3389/fncel.2018.00412>
- Tan, Y. L., Yuan, Y., & Tian, L. (2020). Microglial regional heterogeneity and its role in the brain. *Molecular Psychiatry*, 25, 351–367. <https://doi.org/10.1038/s41380-019-0609-8>
- Tarozzo, G., Bortolazzi, S., Crochemore, C., Chen, S. C., Lira, A. S., Abrams, J. S., & Beltramo, M. (2003). Fractalkine protein localization and gene expression in mouse brain. *Journal of Neuroscience Research*, 73, 81–88. <https://doi.org/10.1002/jnr.10645>
- Tetreault, N. A., Hakeem, A. Y., Jiang, S., Williams, B. A., Allman, E., Wold, B. J., & Allman, J. M. (2012). Microglia in the cerebral cortex in autism. *Journal of Autism and Developmental Disorders*, 42, 2569–2584. <https://doi.org/10.1007/s10803-012-1513-0>
- Trangle, S. S., Rosenberg, T., Parnas, H., Levy, G., Bar, E., Marco, A., & Barak, B. (2023). In individuals with Williams syndrome, dysregulation of methylation in non-coding regions of neuronal and oligodendrocyte DNA is associated with pathology and cortical development. *Molecular Psychiatry*, 28, 1112–1127. <https://doi.org/10.1038/s41380-022-01921-z>
- Tremblay, M. È., & Sierra, A. (2014). *Microglia in health and disease* (p. 486). Springer-Verlag. <https://doi.org/10.1007/978-1-4939-1429-6>
- Tunster, S. J. (2017). Genetic sex determination of mice by simplex PCR. *Biology of Sex Differences*, 8, 31. <https://doi.org/10.1186/s13293-017-0154-6>
- Vidal-Itriago, A., Radford, R. A. W., Aramideh, J. A., Maurel, C., Scherer, N. M., Don, E. K., Lee, A., Chung, R. S., Graeber, M. B., & Morsch, M. (2022). Microglia morphophysiological diversity and its implications for the CNS. *Frontiers in Immunology*, 13, 997786. <https://doi.org/10.3389/fimmu.2022.997786>
- Wang, J., Wang, J., Wang, J., Yang, B., Weng, Q., & He, Q. (2019). Targeting microglia and macrophages: A potential treatment strategy for multiple sclerosis. *Frontiers in Pharmacology*, 10, 286. <https://doi.org/10.3389/fphar.2019.00286>
- Wes, P. D., Holtman, I. R., Boddeke, E. W., Moller, T., & Eggen, B. J. (2016). Next generation transcriptomics and genomics elucidate biological complexity of microglia in health and disease. *GLIA*, 64, 197–213. <https://doi.org/10.1002/glia.22866>
- Wilder, L., Hanson, K. L., Lew, C. H., Bellugi, U., & Semendeferi, K. (2018). Decreased neuron density and increased glia density in the ventromedial prefrontal cortex (Brodmann area 25) in Williams syndrome. *Brain Sciences*, 8, 209. <https://doi.org/10.3390/brainsci8120209>
- Włodarczyk, A., Benmamar-Badel, A., Cédile, O., Jensen, K. N., Kramer, I., Elsborg, N. B., & Owens, T. (2018). CSF1R stimulation promotes increased neuroprotection by CD11c+ microglia in EAE. *Frontiers in Cellular Neuroscience*, 12, 523. <https://doi.org/10.3389/fncel.2018.00523>
- Włodarczyk, A., Cédile, O., Jensen, K. N., Jasson, A., Mony, J. T., Khorrooshi, R., & Owens, T. (2015). Pathologic and protective roles for microglial subsets and bone marrow- and blood-derived myeloid cells in central nervous system inflammation. *Frontiers in Immunology*, 6, 463. <https://doi.org/10.3389/fimmu.2015.00463>
- Włodarczyk, A., Holtman, I. R., Krueger, M., Yogev, N., Bruttger, J., Khorrooshi, R., Benmamar-Badel, A., de Boer-Bergsma, J. J., Martin, N. A., Karram, K., Kramer, I., Boddeke, E. W. G. M., Waisman, A., Eggen, B. J. L., & Owens, T. (2017). A novel microglial subset plays a key role in myelogenesis in developing brain. *The EMBO Journal*, 36, 3292–3308. <https://doi.org/10.15252/emboj.201696056>
- Xie, D., Ge, X., Ma, Y., Tang, J., Wang, Y., Zhu, Y., Gao, C., & Pan, S. (2020). Clemastine improves hypomyelination in rats with hypoxic-ischemic brain injury by reducing microglia-derived IL-1beta via P38 signaling pathway. *Journal of Neuroinflammation*, 17, 57. <https://doi.org/10.1186/s12974-019-1662-6>
- York, E. M., LeDue, J. M., Bernier, L.-P., & MacVicar, B. A. (2018). 3DMorph automatic analysis of microglial morphology in three dimensions from ex vivo and in vivo imaging. *Eneuro*, 5, ENEURO.0266-18. <https://doi.org/10.1523/ENEURO.0266-18.2018>
- Zhan, Y., Paolicelli, R. C., Sforzini, F., Weinhard, L., Bolasco, G., Pagani, F., Vyssotski, A. L., Bifone, A., Gozzi, A., Ragozzino, D., & Gross, C. T. (2014). Deficient neuron-microglia signaling results in impaired functional brain connectivity and social behavior. *Nature Neuroscience*, 17, 400–406. <https://doi.org/10.1038/nn.3641>
- Zusso, M., Methot, L., Lo, R., Greenhalgh, A. D., David, S., & Stifani, S. (2012). Regulation of postnatal forebrain amoeboid microglial cell proliferation and development by the transcription factor Runx1. *The Journal of Neuroscience*, 32, 11285–11298. <https://doi.org/10.1523/JNEUROSCI.6182-11.2012>

## SUPPORTING INFORMATION

Additional supporting information can be found online in the Supporting Information section at the end of this article.

**How to cite this article:** Bar, E., Fischer, I., Rokach, M., Elad-Sfadia, G., Shirenova, S., Ophir, O., Trangle, S. S., Okun, E., & Barak, B. (2024). Neuronal deletion of *Gtf2i* results in developmental microglial alterations in a mouse model related to Williams syndrome. *Glia*, 1–19. <https://doi.org/10.1002/glia.24519>